SUPPLEMENTAL MATERIAL

BOLA3 deficiency controls endothelial metabolism and glycine homeostasis in pulmonary hypertension

Qiujun Yu, Yi-Yin Tai, Ying Tang, Jingsi Zhao, Vinny Negi, Miranda K. Culley, Jyotsna Pilli, Wei Sun, Karin Brugger, Johannes Mayr, Rajeev Saggar, Rajan Saggar, W. Dean Wallace, David J. Ross, Aaron B. Waxman, Stacy G. Wendell, Steven J. Mullett, John Sembrat, Mauricio Rojas, Omar F. Khan, James E. Dahlman, Masataka Sugahara, Nobuyuki Kagiyama, Taijyu Satoh, Manling Zhang, Ning Feng, John Gorcsan III, Sara O. Vargas, Kathleen J. Haley, Rahul Kumar, Brian B. Graham, Robert Langer, Daniel G. Anderson, Bing Wang, Sruti Shiva, Thomas Bertero, and Stephen Y. Chan

Supplemental Methods

Oligonucleotides and transfection

Silencer or Silencer Select siRNAs for BOLA3 (223759), GCSH (145088), HDAC1 (s75), BMPR2 (103303), ENG (s4678), SMAD9 (s8415), CAV1 (s2447), KCNK3 (s7784) and scrambled control (12935300) were utilized (Thermo Fisher Scientific). siRNAs for HIF-1α (sc-35561), HIF-2α (sc-35317) and scrambled control (sc-37007) were utilized (Santa Cruz). Key experiments in cultured PAECs were replicated using a second set (Thermo Fisher Scientific) of BOLA3 (223761), GCSH (14749), and scrambled siRNAs (AM4611) (**Figure S10**). Human PAECs (Lonza) were plated in collagen-coated plastic and transfected 16h later at 70-80% confluence using siRNA (20 nM) and Lipofectamine 2000 reagent (Thermo Fisher Scientific), according to the manufacturers' instructions. RNA or protein was extracted 48 hours post-transfection.

Cell culture and reagents

Primary human and mouse pulmonary arterial endothelial cells (PAECs), human smooth muscle cells (PASMCs), and human adventitial fibroblasts (PAAFs) were grown in basal medium EGM-2, SmGM-2 and FGM-2 supplemented with BulletKit (Lonza), respectively. Fibroblasts derived from a patient with MMDS subtype 2 carrying homozygous missense mutations in BOLA3 were described previously [1]. Experiments were performed at passages 5 to 8. HEK293T cells (American Type Culture Collection) were cultivated in DMEM containing 10% fetal bovine serum (FBS). Recombinant human IL-1β and IL-6 were purchased from Peprotech and used at concentrations of 10ng/ml and 100ng/ml respectively. Valproic acid, dichloroacetate, glycine, and etomoxir were purchased from Sigma Aldrich and used at concentrations of 3 mM, 5 mM, 3 mM and 40 μM, respectively.

Exposure to hypoxia

Primary cells were exposed for 24 hours either to standard non-hypoxic cell-culture conditions, (20% O_2, 5% CO_2, with N_2 balance at 37˚C) or to hypoxia (0.2% O_2, 5% CO_2, with N_2 balance at 37˚C), in a modular hypoxia chamber, as previously described [2]. Conditions were based on prior studies of human PAECs [2] to allow for steady-state adaptation without non-specific cell death.

Plasmids and lentivirus production

The constitutively active HIF-2α plasmid [3] was a kind gift from W. Kim (University of North Carolina, Chapel Hill). The coding sequence of BOLA3 transcript 1 (mitochondrial isoform; Dharmacon, clone ID 4829356) and GCSH were purchased (Dharmacon, Clone ID 3872097) and sub-cloned in the pCDH-CMV-MCS-EF1-copGFP (System Biosciences) using XbaI/EcoRI and XbaI/BamHI restriction sites respectively. All cloned plasmids were confirmed by DNA sequencing. HEK293T cells were co-transfected using Lipofectamine 2000 (Thermo Fisher Scientific) with lentiviral plasmids along with a packaging plasmid system (pPACK, System Biosciences), according to the manufacturer's instructions. Viral particles were harvested 48 hours after transfection, concentrated, sterile filtered (0.45 μm), and lentiviral titers were determined. Human PAECs were then infected at 60-70% confluence (16-24 hours incubation) with polybrene (8 μg/ml) for 2–3 days for gene transduction. The lentiviral parent vector expressing GFP was used as a control. The infection efficiency was assessed in each experiment by observing the GFP expression, which usually ranged from 60% to 80% under a fluorescence microscope.

Messenger RNA extraction and quantitative RT-PCR

RNA extraction and quantitative RT-PCR (RT-qPCR) was performed on an Applied Biosystems Quantstudio 6 Flex Fast Real Time PCR device, as we previously described [4-7]. Fold-change of RNA species was calculated using the formula ($2^{-\Delta\Delta Ct}$), normalized to β-actin expression. Taqman primers are listed in **Table S3**.

ChIP-qPCR

Chromatin precipitation (ChIP) was performed using a magnetic ChIP kit (Pierce) with a few adaptions. Briefly, cells were cross-linked in 1% paraformaldehyde for 10 minutes at room temperature. Fixed cells were lysed in membrane extraction buffer supplemented with 1X protease inhibitor cocktail (Pierce) for 10 minutes on ice. Chromatin after centrifugation was resuspended in IP dilution buffer containing protease inhibitors, and contents were sonicated (Bioruptor) in an ice bath at high power for 20 minutes (20 cycles of 1 minute with 30 seconds on and 30 seconds off). Samples were centrifuged at 20,000 g for 5 minutes, and supernatants containing the soluble chromatin were transferred to fresh tubes for immunoprecipitation. Crosslinked DNA after sonication was precipitated with 5µg of anti-acetylated histone 3 lysine 9 antibody (H3K9Ace, Cell signalling cs9649), anti-HDAC1 (ab7928, Abcam), or non-immune rabbit IgG (Pierce magnetic ChIP kit) overnight at 4°C. Chromatin/antibody complex was pulled down with Protein A/G Magnetic Beads (Pierce) and washed in the low- and high-salt wash buffers. After crosslinking reversion (65°C for 40min) and proteinase K treatment, chromatin was purified by phenol-chloroform extraction and ethanol precipitation. Precipitated DNA was analyzed by qPCR using primers generated for predicted H3K9Ace binding sites in BOLA3 promotor sites or a non-relevant genomic region (Control). ChIP primers are listed in **Table S3**.

Immunoblotting and antibodies

Cells were lysed in Laemmli buffer (Thermo Fisher Scientific). Protein lysates were resolved by SDS-PAGE and transferred onto a PVDF membrane (Biorad). Membranes were blocked in 5% non-fat milk or BSA in PBS buffer containing 0.1% Tween (PBST) and incubated in the presence of the primary at 4°C overnight and then secondary antibodies for 1 hour at room temperature. After washing in PBST buffer, immunoreactive bands were visualized with the ECL system (Amersham Biosciences). Primary antibodies for BOLA3 (LS-C345921, 1/200) and VEGF (SAB1402390, 1/1000) were obtained from LifeSpan Biosciences and Sigma, respectively. Antibody against lipoate (ab58724, 1/1000) was obtained from Abcam. Antibodies against SDHB (sc-25851, 1/200), NOS3 (sc-654, 1/200) and β-actin (sc-47778; 1/5000) were obtained from Santa Cruz Biotechnology. Antibodies against NDUFV2 (NBP1-84475, 1/1000) were obtained from Novusbio. Antibodies against HDAC1 (10197-1-AP, 1/1000), GCSH (16726-1-AP, 1/500), GLDC (24827-1-AP, 1/1000), CPT1A (15184-1-AP, 1/1000), and SHMT1 (14149-1-AP, 1/1000) were purchased from Proteintech. In order to examine phosphorylation state within treated cells, a broad phosphatase inhibitor (PhosSTOP, Sigma) was added to cell lysis buffer cocktail of RIPA and protease inhibitor. Antibodies against p-PDK (3061-S) and PDK1 (3062S) were obtained from Cell Signalling. Appropriate secondary antibodies (anti-rabbit, anti-mouse and anti-goat) coupled to HRP were used (Dako). The density of the bands was quantified by densitometric analysis using the NIH ImageJ sotware (http://rsb.info.nih.gov/ij/).

Fe-S fluorescent sensor quantification

Mammalian expression plasmids encoding GRX2 and GCN4 transgenes fused to the N-terminal or C-terminal portions of the Venus fluorescent protein were provided by Dr. J. Silberg (Rice University), as previously described [8, 9]. Transgenes were subcloned into the pCDH-MCS-EF1-PURO lentiviral parent vector (System Biosciences) via BamHI and NotI sites. Fe-S fluorescent sensor quantification lentiviruses (N-terminal and C-terminal GRX2 constructs mixed in 1:1 v/v ratio; N-terminal and C-terminal GCN4 constructs mixed in 1:1 v/v ratio; and empty lentivirus)

were generated and used for infection of cultured human PAECs in the presence of 2 ug/ml polybrene (Santa Cruz Biotechnology). After 24 hours, viruses were removed, human PAECs were washed with PBS, and EGM-2 media (Lonza) was replaced. Virus-transduced human PAECs were transfected with siRNAs specific for human BOLA3 (20 nM, Thermo Fisher Scientific, 223759) versus control siRNA (20 nM, Thermo Fisher Scientific, 12935300). After 72 hours, fluorescence was imaged by Nikon A1 confocal microscopy. Fe-S content was presented as percentage of PAECs with positive fluorescence.

Endothelin-1 ELISA, PDH activity, lactate assays

Level of excreted endothelin in cell culture media was assessed by endothelin-1 ELISA kit (Enzo Life Sciences), cellular pyruvate dehydrogenase (PDH) activity was measured by colorimetric assay kit (BioVision), and lactate levels in cell lysate/media were measured by colorimetric assay kit (BioVision), according to the manufacturer's instructions.

Mitochondrial complex I activity assay

Assays were performed according to the manufacturer's instructions (Complex I enzyme activity microplate assay kit, Abcam), and as we previously described [2], in treated cells (1-2 × 10^7) or flash frozen mouse lung tissues (100-200 mg/sample).

Glycine assay

According to the manufacturer's instructions (Glycine Assay Kit, BioVision), treated cells (1-2 × 10^6) or flash frozen mouse lung tissues (10-20 mg/sample) was homogenized in 100µl of glycine assay buffer on ice and centrifuged at 10,000g 4°C for 5 min. Supernatants were collected and protein concentrations were determined by Bradford assay. Samples were

incubated with kit reagents for 1 hr at 25°C protected from light, and fluorescence (Ex/Em=535/587 nm) was measured in end point mode and normalized to protein content.

High resolution liquid chromatography mass spectrometry (LC-HRMS)

Sample preparation: metabolic quenching was performed on 6 × 10^5 human PAECs on dry ice using 80% aqueous methanol pre-cooled at -80°C. The polar metabolite pool was extracted using $CHCl_3$:MeOH:H_2O (2:1:1). 40 µL of internal standard, U-^{13}C, 98%+ lyophilized algal cells (Cambridge Isotope Laboratories) was added during metabolite extraction. The polar phase was separated at 1,500 x g for 5 minutes at 4°C. The supernatant was dried under nitrogen gas and resuspended in 100 µL 5% aqueous acetonitrile with 0.1% formic acid.

Untargeted LC-HRMS were performed using a modified version of a three-minute gradient, as previously published [10]. Briefly, samples were resolved under isocratic 0.2 mL/min flow in 5% aqueous acetonitrile with 0.1% formic acid over a Thermo Fisher Accucore Vanquish C18+ column (2.1 × 100 mm, 1.5 µm particle size). The Q Exactive mass spectrometer was operated in negative ion mode, scanning in Full MS mode (2 µscans) from 60 to 900 *m/z* at 70,000 resolution with an AGC target of 3 × 10^6. Source settings were 4.5 kV spray voltage, 20 sheath gas, 10 auxiliary gas at 250°C, and 4 sweep gas. Calibration was performed prior to analysis using the Pierce™ Negative Ion Calibration Solutions (Thermo Fisher Scientific). Integrated peak areas were then extracted manually using Quan Browser (Thermo Fisher Xcalibur ver. 2.7).

Seahorse assay

In PAECs (20,000 cells/well), oxygen consumption rate and extracellular acidification rate (a surrogate marker of glycolysis) were measured on an XFe96 Extracellular Flux Analyzer

(Seahorse Biosciences) by sequential addition of 1uM Oligomycin, 0.5uM FCCP, and 2uM Rotenone plus 0.5uM Antimycin, as we previously described [7]. Etomoxir (40 μM), a CPT-1 (carnitine palmitoyl transferase-1) inhibitor, was added 15 minutes prior to the assay in a separate experiment to block fatty acid uptake by the mitochondria. In a parallel study using XF Palmitate-BSA FAO Substrate (Seahorse Bioscience), growth medium was replaced with substrate-limited medium (0.5 mM glucose, 1 mM GlutaMAX, 0.5 mM carnitine and 1% FBS) 24 hours prior to the assay. Cells were washed once with FAO Assay Medium (KHB supplemented with 0.5 mM glucose, 0.5 mM carnitine, and 5 mM HEPES) 45 minutes prior to the assay and incubated in 135 μL/well FAO assay medium for 30 minutes at 37°C. Then Etomoxir (40 μM) was added to FAO Assay Medium in appropriate cells and incubate for 15 minutes at 37°C. XF Palmitate-BSA FAO Substrate (30 μL/well) was added immediately prior to assay.

Cell counting assay, BrdU proliferation assay, caspase 3/7 assay

All assays were performed as we previously described [4-7] and per the manufacturers' instructions [BrdU Cell Proliferation Assay Kit (6813, Cell Signaling); Caspase-Glo 3/7 Assay (Promega)]. For the caspase 3/7 assay, PAECs (10,000 cells/well) were incubated with Caspase-Glo 3/7 reagent in 96-well plate at room temperature for 1 hour, luminescence was recorded and normalized to protein content, as measured by BCA assay.

Wound healing scratch assay

Confluent PAECs were wounded using pipet tips and wound bed closures were followed serially over 12 hours. Brightfield images were captured every 4 hours using EVOS XL CORE imaging system (Life Technologies). Wound bed areas were quantified using the NIH ImageJ software (http://rsb.info.nih.gov/ij/).

In vitro angiogenesis assays

Capillary tube formation was performed using a commercial kit (*In vitro* angiogenesis assay kit, Cultrex, #3470-096-K). Briefly, Matrigel with reduced growth factors was pipetted into pre-chilled 96-well plate (50 µl Matrigel per well) and polymerized for 30 min at 37°C. HPAECs following different treatments (2×10^4 cells per well) were stained with Calcein AM (Cultrex, 1µM) for 30 min at 37°C, resuspended in 100 µl of basic media, and seeded in Matrigel coated 96-well plate. After 4-6 h of incubation, tubular structures were photographed using Olympus inverted fluorescent microscope with a 20× magnification. The number of branch points was quantified in triplicate determinations from 3 separate experiments.

In vivo angiogenesis assay

An *in vivo* Matrigel plug angiogenesis assay was performed, following a previously described protocol [11, 12] with modifications. Human PAECs were transfected with BOLA3 siRNA (223759, Thermo Fisher Scientific) or scrambled RNA control (12935300, Thermo Fisher Scientific). At 24 hours after transfection, 1×10^6 cells were mixed with 400 µl Matrigel (Corning) containing 30 units/ml heparin and 40 ng/ml basic fibroblast growth factor (Thermo Fisher Scientific), which was then injected subcutaneously into the dorsal surface of SCID male mice (10-12 weeks old, Jackson Lab). The mice were kept under normoxic condition (21% O_2) for 5 days. After euthanasia, Matrigel plugs were harvested and photographed. For hemoglobin quantification, Matrigel plugs were homogenized in 200 µl distilled deionized water. Hemoglobin level in the supernatant after centrifugation was then determined using a Hemoglobin Colorimetric Assay Kit (Cayman Chemical). For histology, Matrigel plugs were embedded in OCT. The frozen sections were prepared for confocal microscopic staining in the following manner: the OCT-embedded Matrigel sections were incubated with rat anti-mouse CD31 antibody (Abcam, 1:100 dilution) overnight at

4°C, then incubated with fluorescence labeled rabbit anti-rat IgG secondary antibody (Thermo Fisher Scientific, 1:200 dilution) for 1 hour at room temperature, followed by 4′,6-diamidino-2-phenylindole dye (DAPI) staining for cell nucleus. The sections were imaged under fluorescence microscope (EVOS FL Imaging System, Thermo Fisher Scientific) and quantified for CD31+ cells.

Contraction and co-culture assays

PASMCs (50,000/well) were embedded in 100 μl of matrix gel and plated into a 96-well plate as described previously [13]. Briefly, cells were embedded in a mixture of growth factor reduced Matrigel (BD Biosciences) and collagen-I (BD Biosciences). Collagen-I solution was neutralized on ice with 0.1 M NaOH in PBS and adjusted with 0.1 N HCl to bring the pH of the solution to 7.5. The collagen-I solution was then mixed on ice with Matrigel to obtain a final concentration of 1.5 mg/ml. Cells were trypsinized, counted, and resuspended in growth medium; then 1 volume of cells was mixed with 1 volume of the ECM mix. After 1 h at 37 °C, these matrices were overlaid with 100 μl of conditioned PAEC serum-free medium (transfected with siRNA or transduced with lentiviruses). Every 12 h, medium was changed, and at day 4, the gels were photographed, followed by measurement of the relative diameter of the well and the gel using ImageJ software. The percentage contraction was calculated as 100 × (well diameter - gel diameter)/well diameter.

Mitochondrial O_2^- and membrane potential measurements

Mitochondrial O_2^- and membrane potential were detected by MitoSox red and Tetramethylrhodamineester (TMRE), respectively. Briefly, cells were incubated with 5 μmol/L Mitosox red (Molecular Probes M36008) or 200 nmol/L TMRE (Molecular Probes T669) for 20 minutes at room temperature. Mitochondria was counterstained by Mitotracker green, which is a hydrophilic dye that accumulates specifically in the mitochondrial membrane regardless of

membrane potential (100nmol/L, Molecular Probes M7514). The cells were then washed 3 times and fixed with 4% of paraformaldehyde, and images were obtained with Zeiss fluorescence microscopy. The intensity of the fluorescence was quantified by NIH Image J software and normalized to Mitotracker green.

Amplex red H_2O_2 assay

Intracellular H_2O_2 was measured by Amplex red assay (Invitrogen A22188). 48 h following siRNA transfection, HAPECs were washed twice with Dulbecco's phosphate-buffered saline (dPBS) and incubated with dPBS containing Amplex Red (50 μM), horseradish peroxidase (0.1 U/ml) and superoxide dismutase (10 U/ml) for 30 min in the dark. Fluorescence intensity was determined in cell supernatants at 530 nm excitation and 590 nm emission wavelengths and normalized to protein contents.

***In situ* 8-oxoguanine staining**

The cells were cultured on Lab-Teck chamber slide (Falcon Co. Ltd., Meylan, France) and were fixed with 4% paraformaldehyde. To prevent the elimination of 8-oxo-dGTP, slides were incubated with RNase for 1 h and with proteinase K for 7 min at room temperature. After blocking the nonspecific binding with serum, slides were incubated with mouse monoclonal antibody against 8-oxoguanine (sc-130914, Santa Cruz) overnight at 4°C. After rinsed 3 times with PBS, the targeted antigens in the cells were detected with Alexa Fluor 488-conjugated anti-mouse IgG antibody (Molecular Probes). Nuclear staining was performed with 4′,6-diamidino-2-phenylindole dye (DAPI). Cells were imaged with a Nikon A1 confocal microscope.

Rodent models of PH

In situ expression/histologic analyses of rodent tissue, and pulmonary vascular hemodynamics in mice and rats were performed in a blinded fashion.

Chronic hypoxic exposure in mice: To elicit chronic hypoxic PH, C57BL/6 WT littermate male and female mice (10-12 weeks old, JAX) were subjected to 21-28 continuous days of normobaric hypoxia in a temperature-humidity controlled chamber (10% O_2, OxyCycler chamber, Biospherix Ltd.) as compared with normoxia (21% O_2). At 3-4 weeks post-exposure, non-invasive tail plethysmography of systemic blood pressure was performed by the CODA system (Kent Scientific) as previously described [6], per the manufacturer's instructions and after acclimating mice to the apparatus. Right heart catheterization was performed followed by harvest of lung tissue for RNA and protein extraction and OCT embedding, as described below.

Bleomycin administration and chronic hypoxia in mice: To elicit a model of severe pulmonary fibrosis relevant to human Group 3 PH utilizing a combination of bleomycin exposure and hypoxia [14], C57BL/6 WT littermate male and female mice (10-12 weeks old, JAX) were subjected to oropharyngeal aspiration of 0.035U of bleomycin (B8416-15un, Sigma) followed by 21 days of normobaric hypoxia (10% O_2). Post-exposure prior to euthanasia, right heart catheterization and tissue harvest were performed. Assessment of pulmonary collagen I and III transcript expression of lung tissues via RT-qPCR and *in situ* staining (Ashcroft scoring) for α–smooth muscle actin were used as quantitative markers of fibrosis. Ashcroft scoring was also used as a surrogate for pulmonary vascular remodeling.

Pulmonary interleukin-6 (IL-6) transgenic mice in hypoxia: To elicit a model of pulmonary inflammation resulting in severe PH, C57BL/6 IL-6 transgenic male mice [15] (10-12 weeks old) were subjected to 21 days of normobaric hypoxia (10% O_2). Non-invasive tail cuff measurement of systemic blood pressure was performed post-exposure, followed by right heart catheterization and tissue harvest as previously described.

S. mansoni infection in mice: Exposure of C57BL/6 WT male mice (10-12 weeks old, Taconic) to *S. mansoni* ova to cause experimental PH was performed using published techniques [16] and

previously described by our group [6]. Upon completion of each of these protocols to induce experimental PH, a combination of non-invasive tail cuff assessment of systemic blood pressure, right heart catheterization, euthanasia, and tissue harvest was performed as described previously [6].

Monocrotaline exposure in rats: As we previously described [6], male Sprague-Dawley rats (10-14 week old) were injected with 60 mg/kg monocrotaline. Prior to euthanasia, right heart catheterization was performed, followed by invasive catheterization of the abdominal aorta to quantify systemic blood pressure. Thereafter, lung tissues were paraffin embedded via an ethanol-xylene dehydration series, before being sliced into 5μm sections (Hypercenter XP System and Embedding Center, Shandon).

SU5416+hypoxia exposure in rats: Male Sprague-Dawley rats (10-14 week old, Charles River) were injected with 20 mg/kg SU5416 (Sigma) followed by 3 weeks of normobaric hypoxia (10% O_2). Prior to euthanasia, right heart catheterization was performed, followed by invasive catheterization of the abdominal aorta to quantify systemic blood pressure. Thereafter, lung tissues were paraffin embedded via an ethanol-xylene dehydration series, before being sliced into 5μm sections (Hypercenter XP System and Embedding Center, Shandon).

In vivo supplementation of glycine in mice: According to the manufacturer's instructions, mini-osmotic pumps (Model 2002, Alzet) were used with a total volume of 200ul and a capacity for a consistent diffusion rate of 0.5ul per hour for a duration of 2 weeks. Based on calculations and maximum solubility of glycine (24.99g/100mL) in saline, mini pumps containing 200μl of saline or 23% glycine (Sigma) were implanted subcutaneously on the backs on C57BL/6 WT littermate male mice (12-14 weeks old), immediately followed by exposure to 10% hypoxia or normoxia for a duration of 2 weeks. During the course of 2 weeks, 0.25% of glycine (Sigma) was also supplemented in the drinking water as compared with saline supplementation. Upon completion of hypoxic exposure and glycine supplementation, non-invasive echocardiography, tail cuff measurement of systemic blood pressure, and right heart catheterization were performed. Lung

tissues were flash frozen in liquid nitrogen for RNA and protein and OCT embedded for *in situ* staining as described below.

Generation and delivery of anti-BOLA3 oligonucleotide:7C1 particles

The nanoparticle 7C1, composed of low molecular weight polyamines and lipids, was utilized for endothelial-specific delivery of BOLA3 siRNA in mice [17], as described [9]. Mice received tail-vein intravenous doses of BOLA3 siRNA (Stealth siRNA MSS294245, Thermo Fisher Scientific, 1mg/kg) or scramble control siRNA (Stealth siRNA Medium GC, Thermo Fisher Scientific, 1mg/kg) formulated in 7C1 with 4 day intervals from day 1 (day 1, 5, 9, 13, 17, 21, 25). Right heart catheterization and echocardiography were performed on day 28.

Generation and delivery of rAAV6-BOLA3 vector

Mouse BOLA3 coding sequence (Dharmacon, ID40126266) or GFP was cloned into a double-stranded rAAV6 backbone carrying a constitutive CMV promoter [18]. The transduction and expression efficiencies of rAAV serotypes 2, 5, 6, 8, 9 were tested in culture mouse pulmonary endothelial cells. rAAV6 viruses were generated by triple plasmid co-transfection of 293 cells and purified twice with cesium chloride gradient ultracentrifugation according to a previously published protocol [19]. Vector titers [5×10^{12} genome copy number per ml (v.g./mL)] were determined using DNA dot-blot hybridization. Mice were anesthetized by inhaled isoflurane with oxygen using a precision vaporizer (induced at 3%, maintained at 1.5–3%) in a closed ventilation chamber, followed by orotracheal instillation of 100μl aliquots of rAAV6-BOLA3 or rAAV6-GFP control.

Rodent echocardiography, non-invasive tail cuff plethysmography, and right heart catheterization

Echocardiography was performed using a 15-45MHz transthoracic transducer and a VisualSonics Vevo770 system (Fujifilm). Inhaled isoflurane anesthesia was used at 2% in 100% O_2 during positioning and hair removal and then decreased to isoflurane 0.8% during imaging. Digital echocardiograms were analyzed off-line for quantitative analysis as previously described [6]. Non-invasive tail cuff plethysmography and subsequent right heart catheterization were performed as previously described [6].

Isolation of mouse pulmonary vascular endothelial cells

Pulmonary vascular endothelial cells were isolated as we previously reported [6]. The purity (>95%) of CD31-positive cells was confirmed by flow cytometric analysis by a FACScan flow cytometer (BD Biosciences) after cell labelling with the FITC-conjugated anti-CD31 (ab33858, Abcam).

Tissue harvest of mouse lungs

After physiological measurements described above, organs were harvested and prepared as previously described [7]. Further molecular assays and in situ staining were performed on representative subsets of harvested tissue, based on availability of samples.

Immunohistochemistry and immunofluorescence of lung sections

Cryostat sections were cut from OCT embedded lung tissues at 5-10 μm and mounted on gelatin-coated histological slides. Slides were thawed at room temperature for 10-20 min and rehydrated in wash buffer for 10 min. All sections were blocked in 10% donkey serum and exposed to primary antibody and Alexa 488, 568 and 647-conjugated secondary antibodies (Thermo Fisher Scientific) for immunofluorescence. Primary antibody against BOLA3 (NBP2-30607; 1/200) and cleaved caspase-3 (cs-9661; 1:400) were obtained from Novus biologicals

and Cell Signaling, respectively. Primary antibodies against lipoate (ab58724, 1/200), CD31 (ab7388,1/200), and PCNA (ab156876, 1/100) were obtained from Abcam. Antibody against α-SMA (F3777; 1/200) and GCSH (sc-242901, 1/100) were purchased from Sigma and Santa Cruz Biotechnology, respectively. Pictures were obtained using Nikon A1 confocal microscopy. Small pulmonary vessels (<100 μm diameter) present in a given tissue section (>10 vessels/section) that were not associated with bronchial airways were selected for analysis. Intensity of staining was quantified using ImageJ software (NIH). Degree of pulmonary arteriolar muscularization was assessed in OCT lung sections stained for α–SMA by calculation of the proportion of fully and partially muscularized peripheral (<100 μm diameter) pulmonary arterioles to total peripheral pulmonary arterioles, as previously described [6]. As previously described [6], medial thickness was also measured in α-SMA stained vessels (<100 μm diameter) using ImageJ software (NIH) and expressed as arbitrary units. All measurements were performed blinded to condition.

For scoring pathologic pulmonary fibrosis, lung OCT sections (5um) were fixed in PBS/PFA 3% 10 min at room temperature and washed twice in PBS 1X, followed by blocking in TBS/BSA 5%, 10% goat serum and exposure to primary antibody and biotinylated secondary antibody (Vectastain ABC kit, Vector Labs). A primary antibody against α-SMA (1/400) was purchased from Abcam. Color development was achieved by adding streptavidin-biotinylated alkaline phosphatase complex (Vector Labs) followed by Vector Red alkaline phosphatase substrate solution (Vector Labs). Levamisole was added to block endogenous alkaline phosphatase activity (Vector Labs). Pictures were obtained using an Axio Observer Z1 motorized inverted microscope (Zeiss). 10 random 10x fields per animal were analyzed. Degree of pulmonary fibrosis was assessed in lung sections stained for α-SMA by Ashcroft score [20], as we have used previously [5]. Ashcroft scoring was also used as a surrogate for pulmonary vascular remodeling.

Supplemental Tables

Supplemental Table 1. Clinical characteristics of PAH patients used for *in situ* staining

Age	Gender	mPAP (mmHg)	Diagnosis	Clinical description
34	Female	50	Idiopathic	Cardiopulmonary arrest (autopsy)
64	Female	55	Idiopathic	Cardiopulmonary arrest (autopsy)
68	Female	44	Scleroderma	Bilateral lung transplant
12	Male	53	BMPR2 mutation	Bilateral lung transplant
16	Male	62	Idiopathic	Bilateral lung transplant
1	Male	50	Trisomy 21	Lung resection
19	Male	48	Idiopathic	Lung resection
42	Female	57	Scleroderma	Bilateral lung transplant

Mean pulmonary arterial pressure (mPAP)

Supplemental Table 2. Clinical characteristics of Group 3 PH patients used for *in situ* staining

Age	Gender	mPAP (mmHg)	Diagnosis	Clinical description
62	Male	28	IPF and PH	Bilateral lung transplant
58	Male	28	IPF and PH	Bilateral lung transplant
63	Male	27	IPF and PH	Bilateral lung transplant
50	Male	30	IPF and PH	Bilateral lung transplant
61	Male	37	IPF and PH	Bilateral lung transplant
69	Female	29	IPF and PH	Bilateral lung transplant
72	Male	46	IPF and PH	Rapid autopsy
66	Male	34	IPF and PH	Bilateral lung transplant

Mean pulmonary arterial pressure (mPAP)

Supplemental Table 3. TaqMan gene expression assays and ChIP primers

Human BOLA3	Hs00918273_g1	Human LDHA	Hs01378790_m1
Human PDK1	Hs01561847_m1	Human GCSH	Hs01631566_g1
Human CPT1A	Hs00912671_m1	Human NRF1	Hs00602161_m1
Human TFAM	Hs00273372_s1	Human Actin	Hs99999903_m1
Mouse Col1a1	Mm00801666_g1	Mouse Col3a1	Mm00802300_m1
Mouse Actin	Mm00607939_s1		
CHIP_AcetyHis_BOLA3_1_For		CCTCCTCCAAATCCCACACT	
CHIP_AcetyHis_BOLA3_1_Rev		ATGATCACTGTCCACGCTGA	
CHIP_AcetyHis_BOLA3_2_For		CCCTCATCCGAATACCCCTC	
CHIP_AcetyHis_BOLA3_2_Rev		GGAGCGATCTTTCTCAAGCG	
CMV promoter_For		CAAGTACGCCCCCTATTGAC	
CMV promoter_Rev		TATCCACGCCCATTGATGTA	

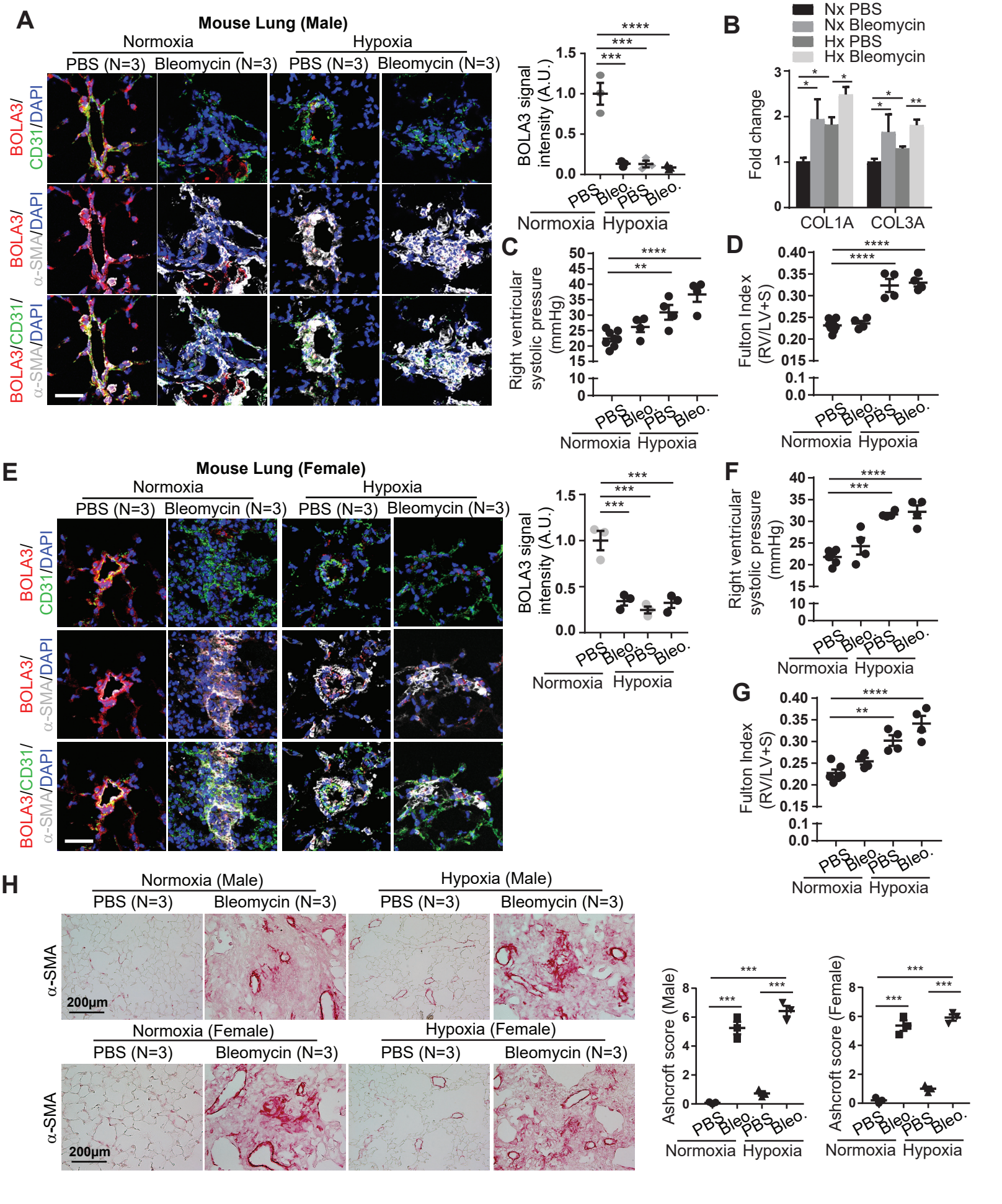

Yu et al. Figure S1

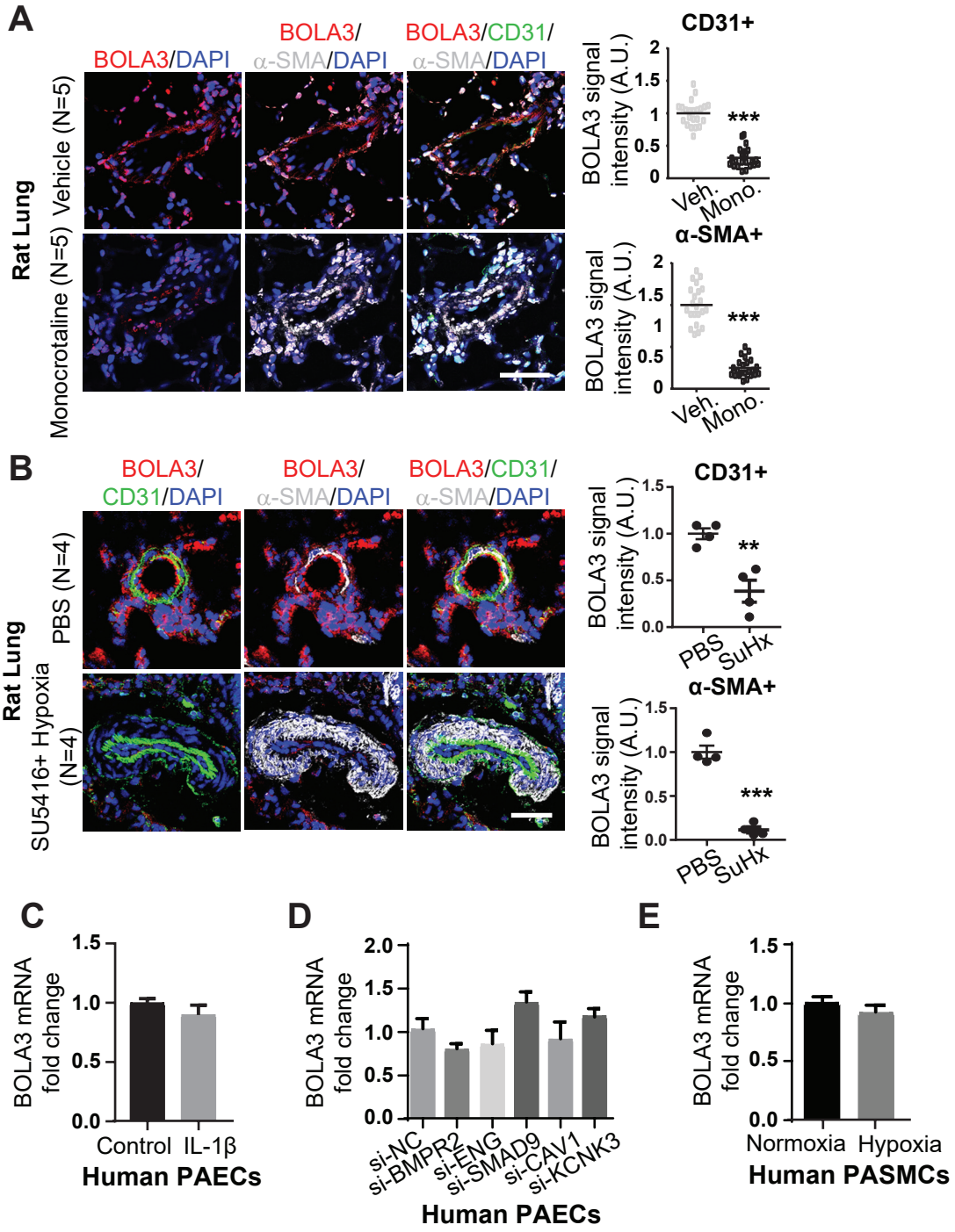

Yu et al. Figure S2

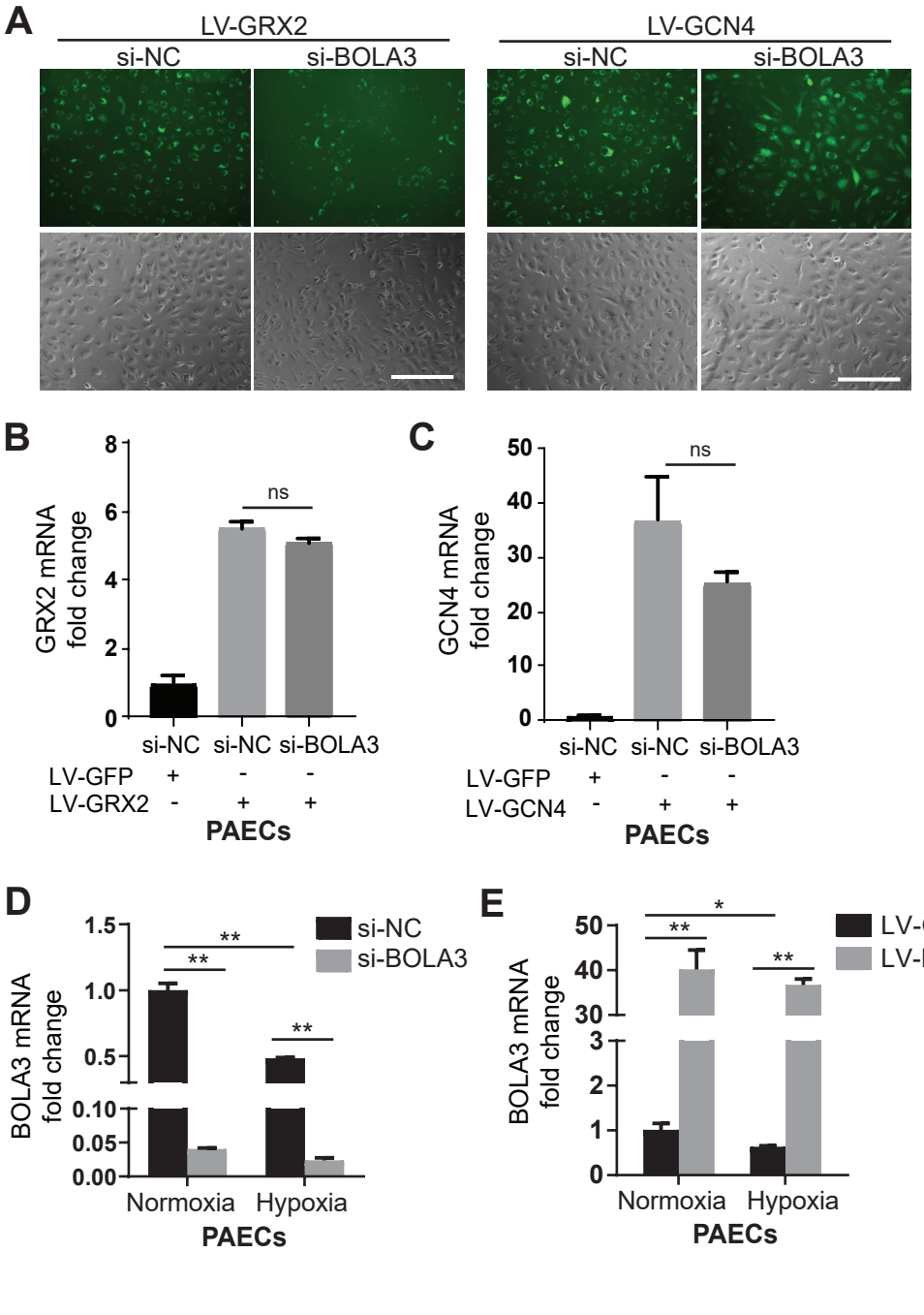

Yu et al. Figure S3

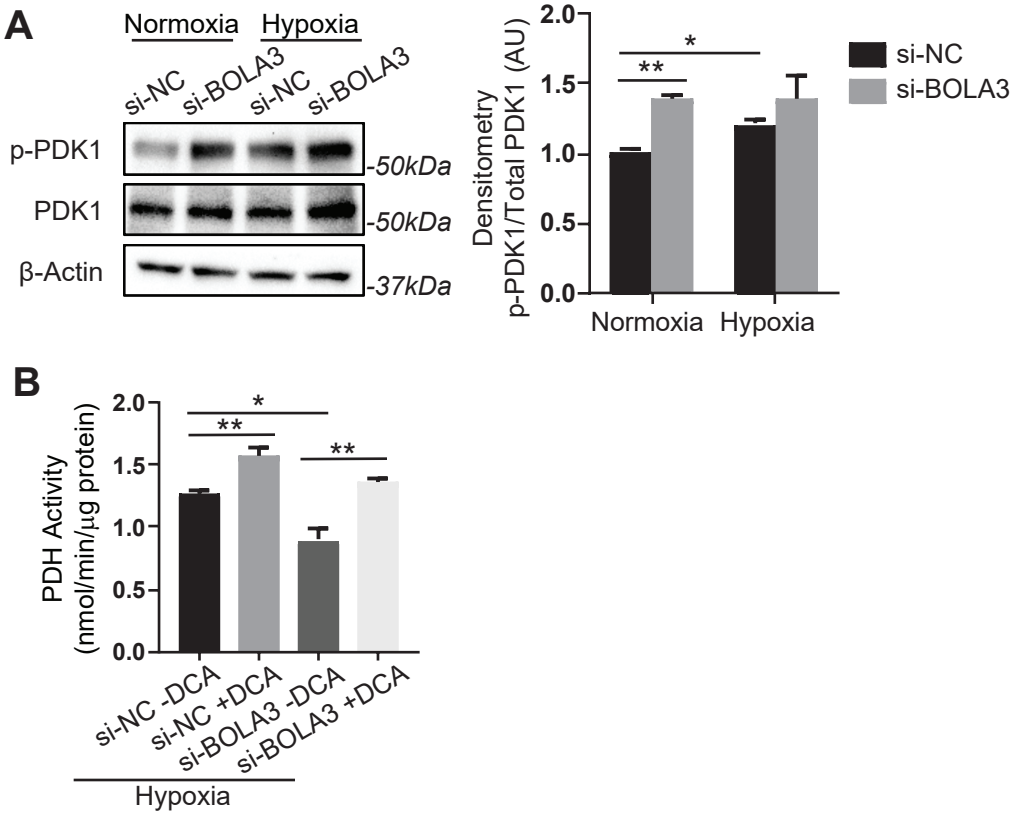

Yu et al. Figure S4

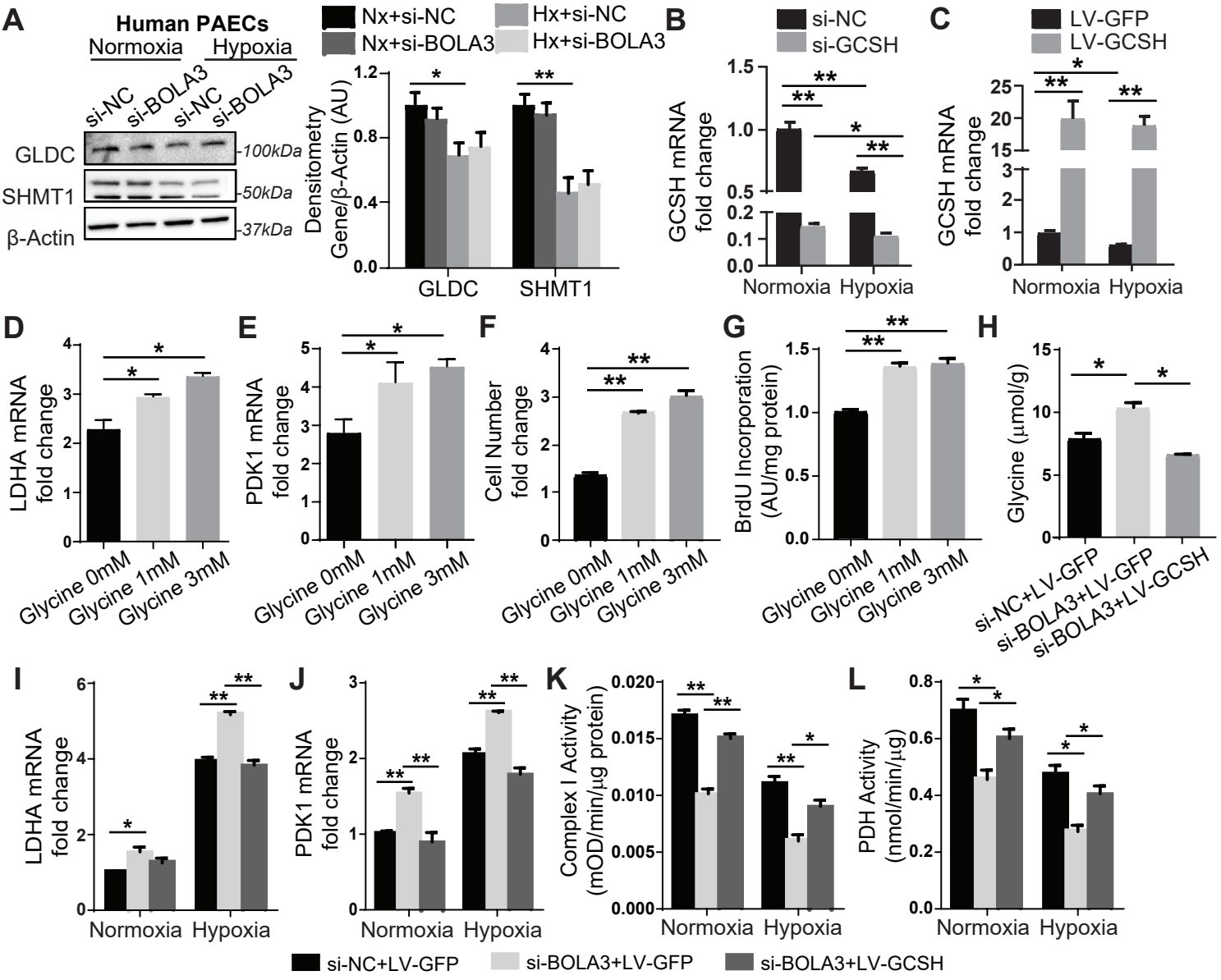

Yu et al. Figure S5

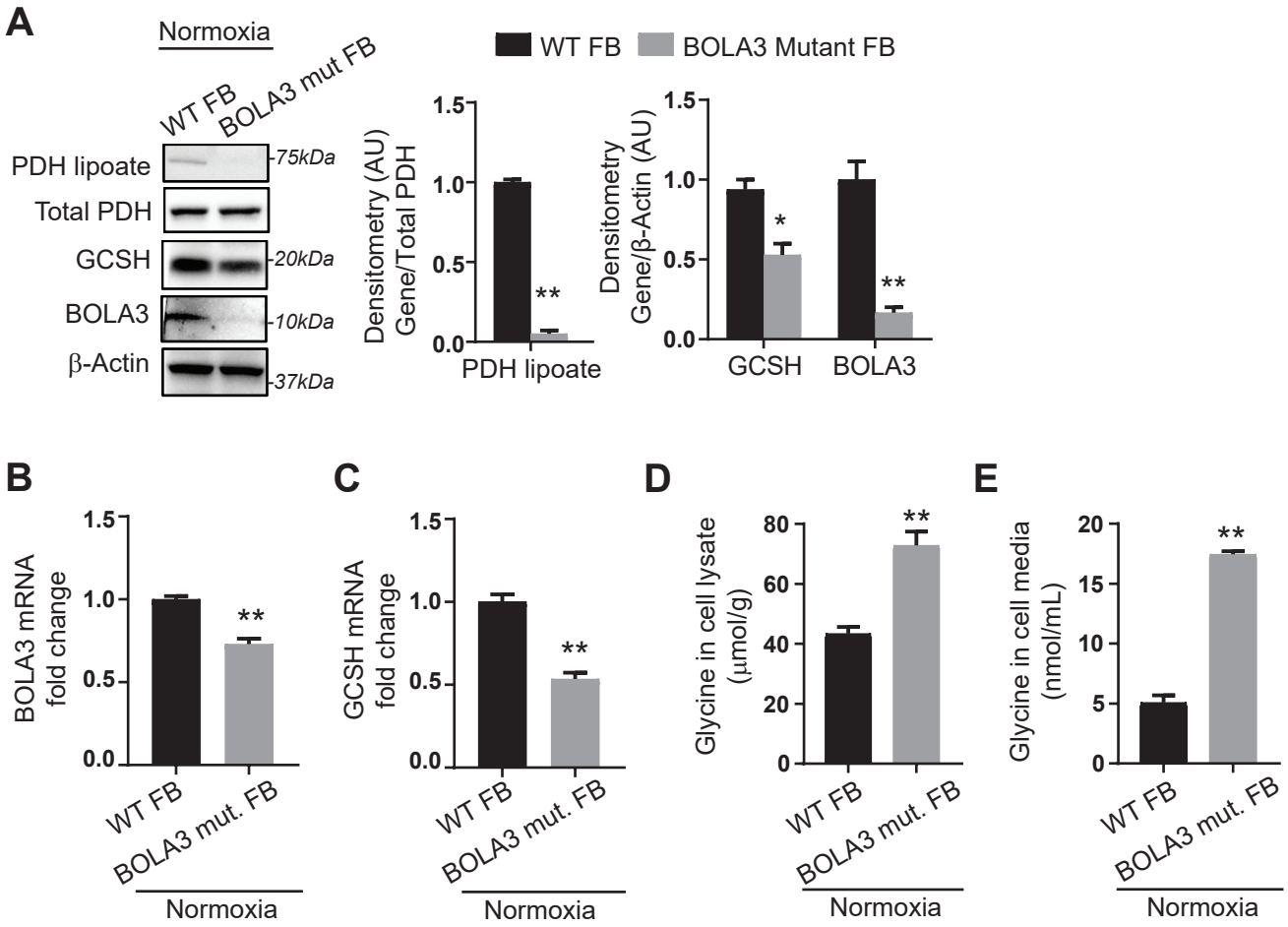

Yu et al. Figure S6

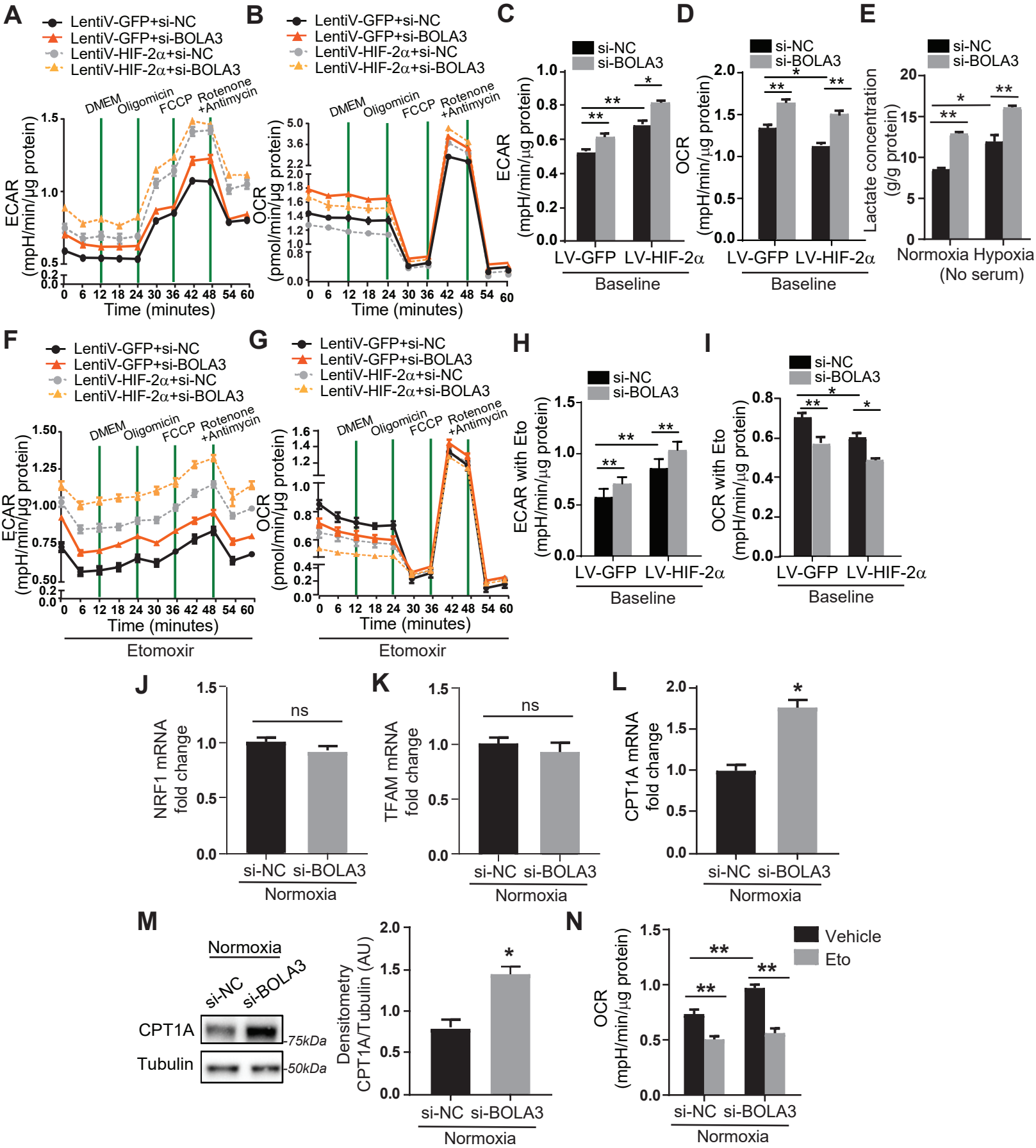

Yu et al. Figure S7

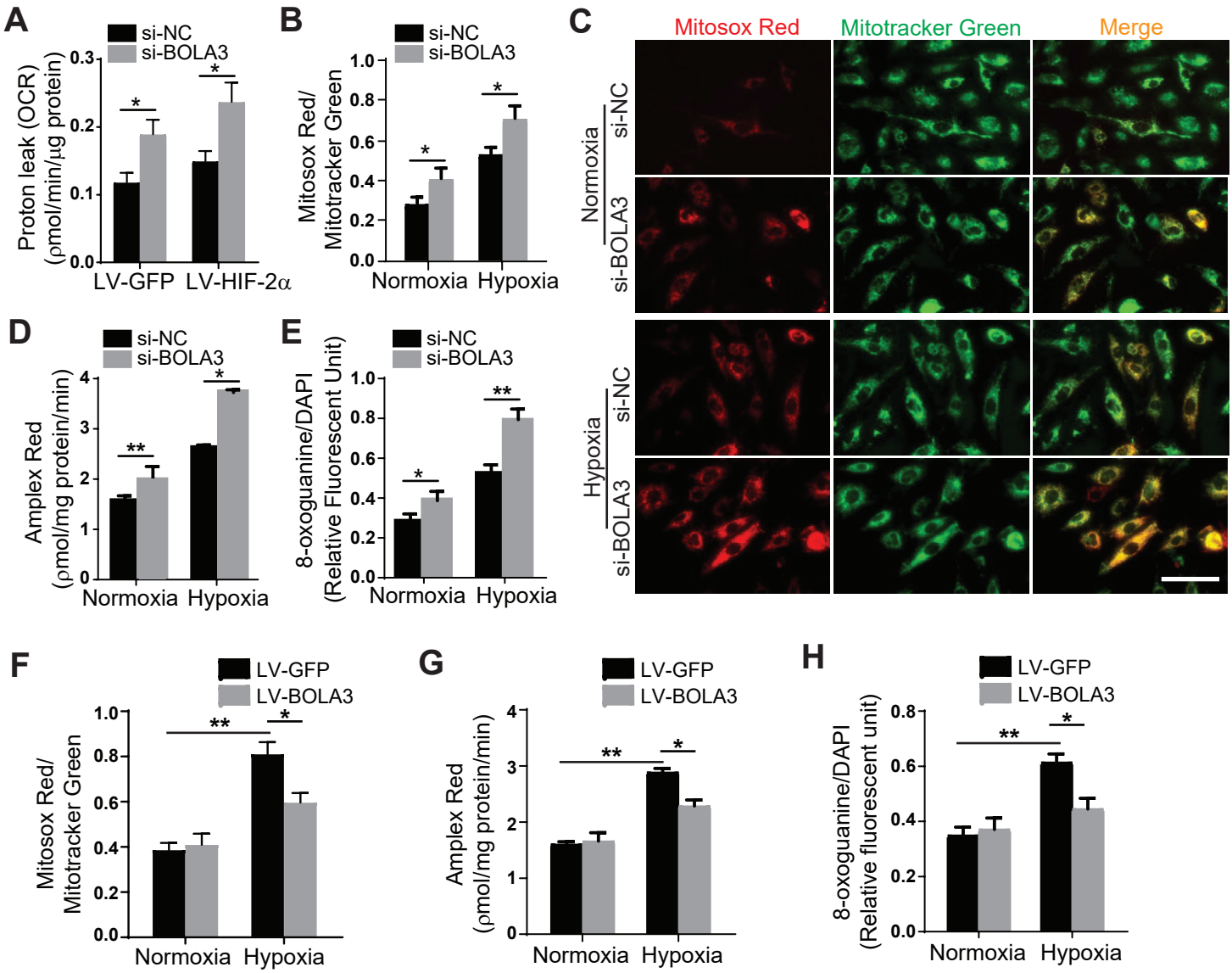

Yu et al. Figure S8

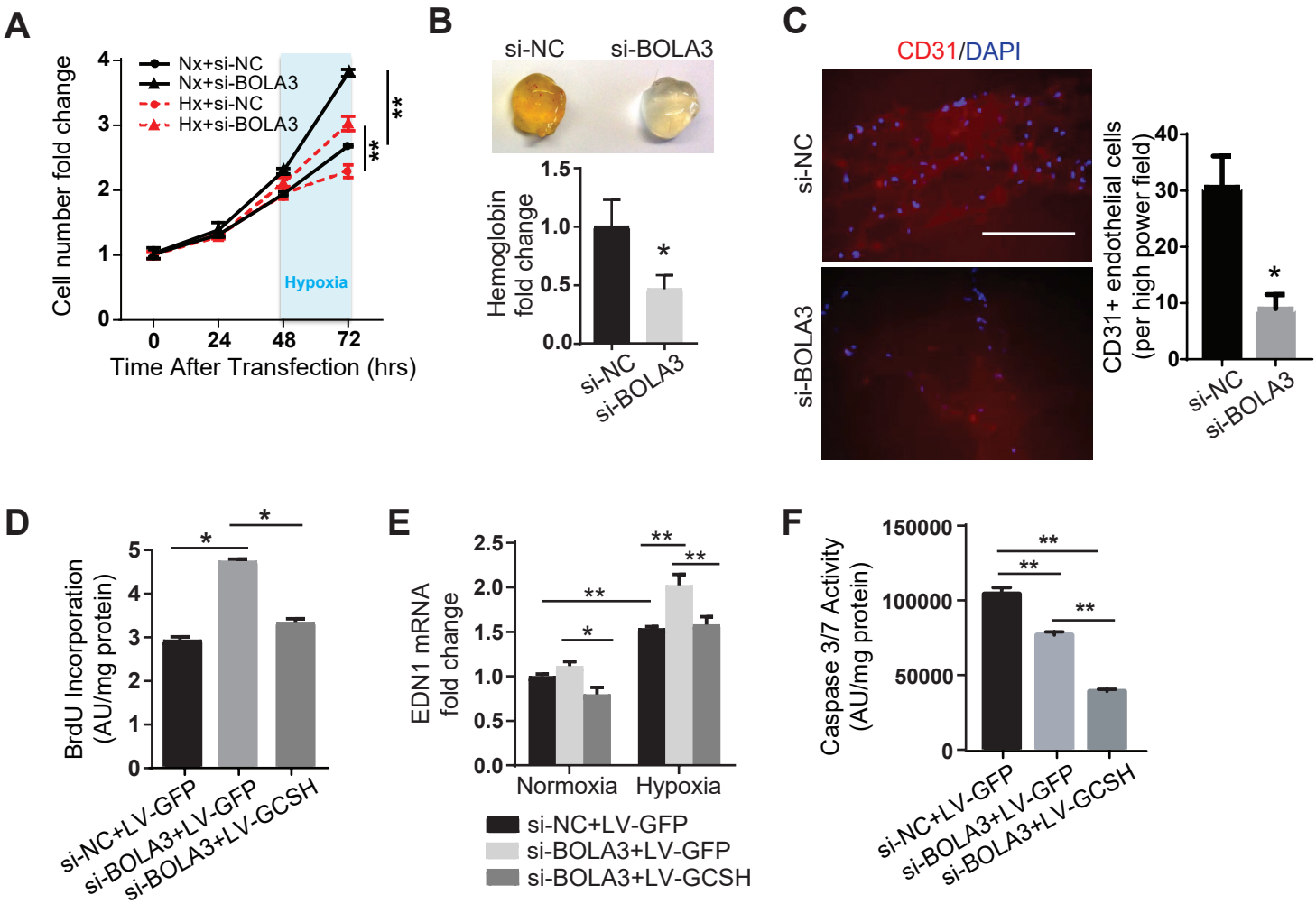

Yu et al. Figure S9

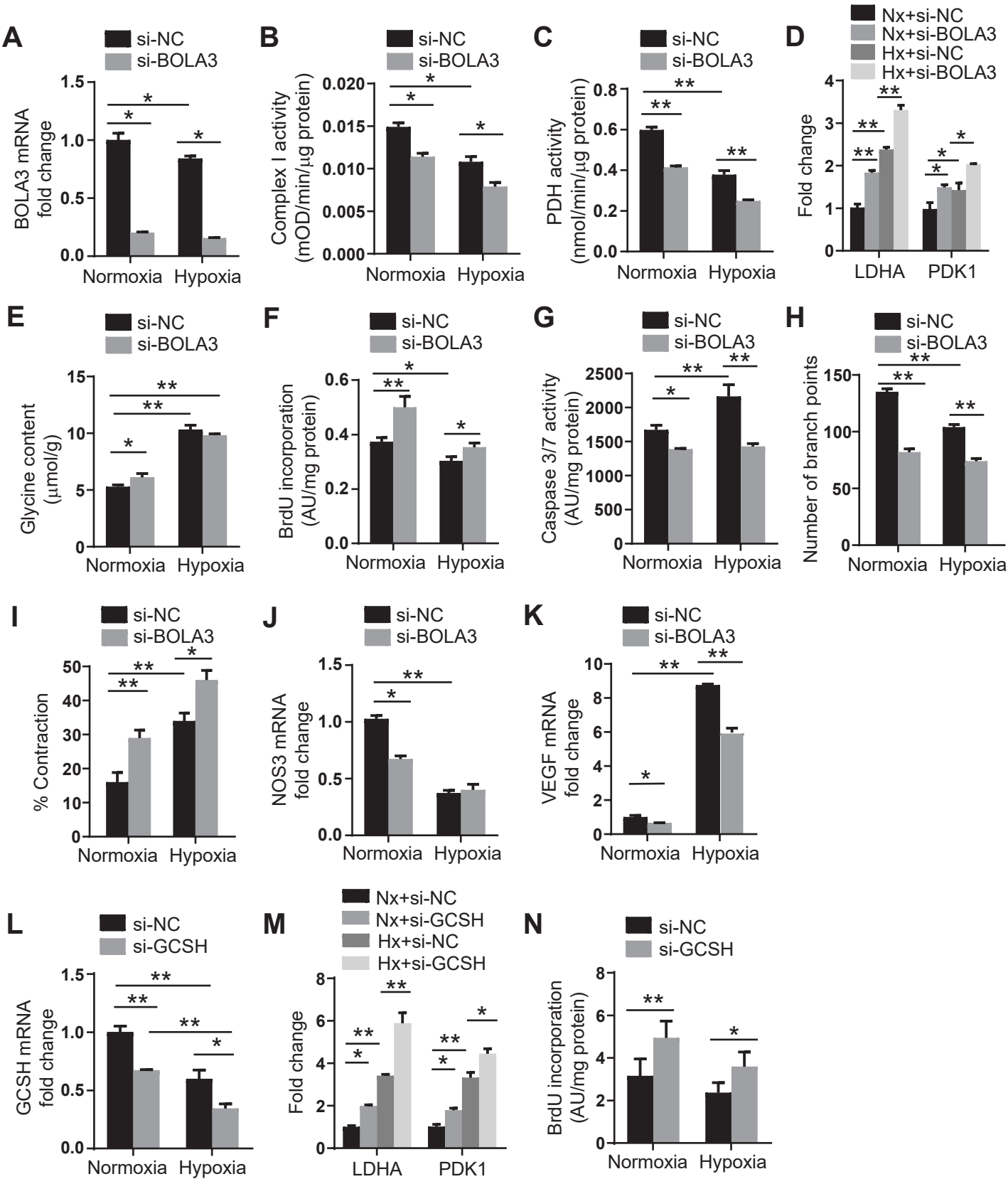

Yu et al. Figure S10

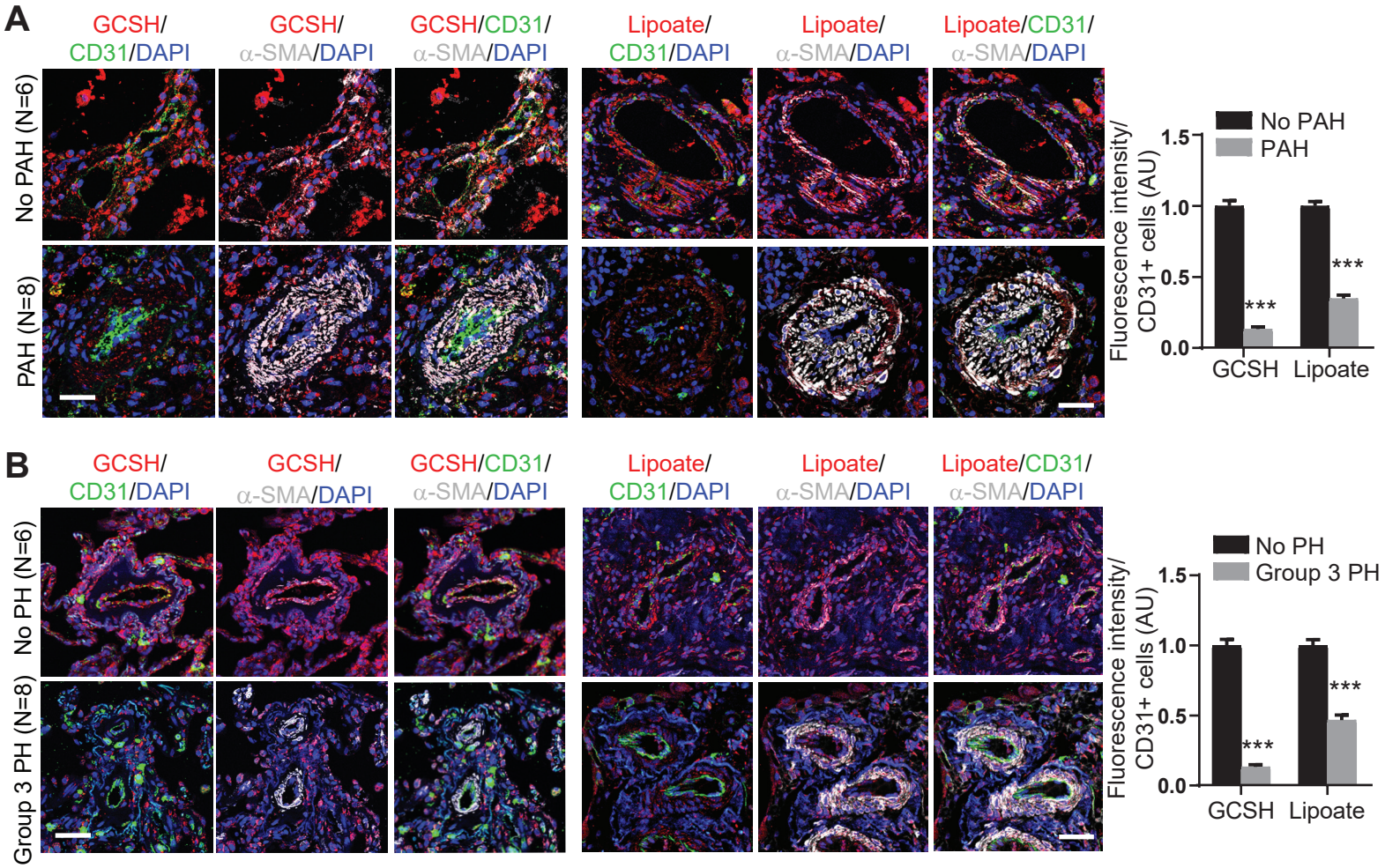

Yu et al. Figure S11

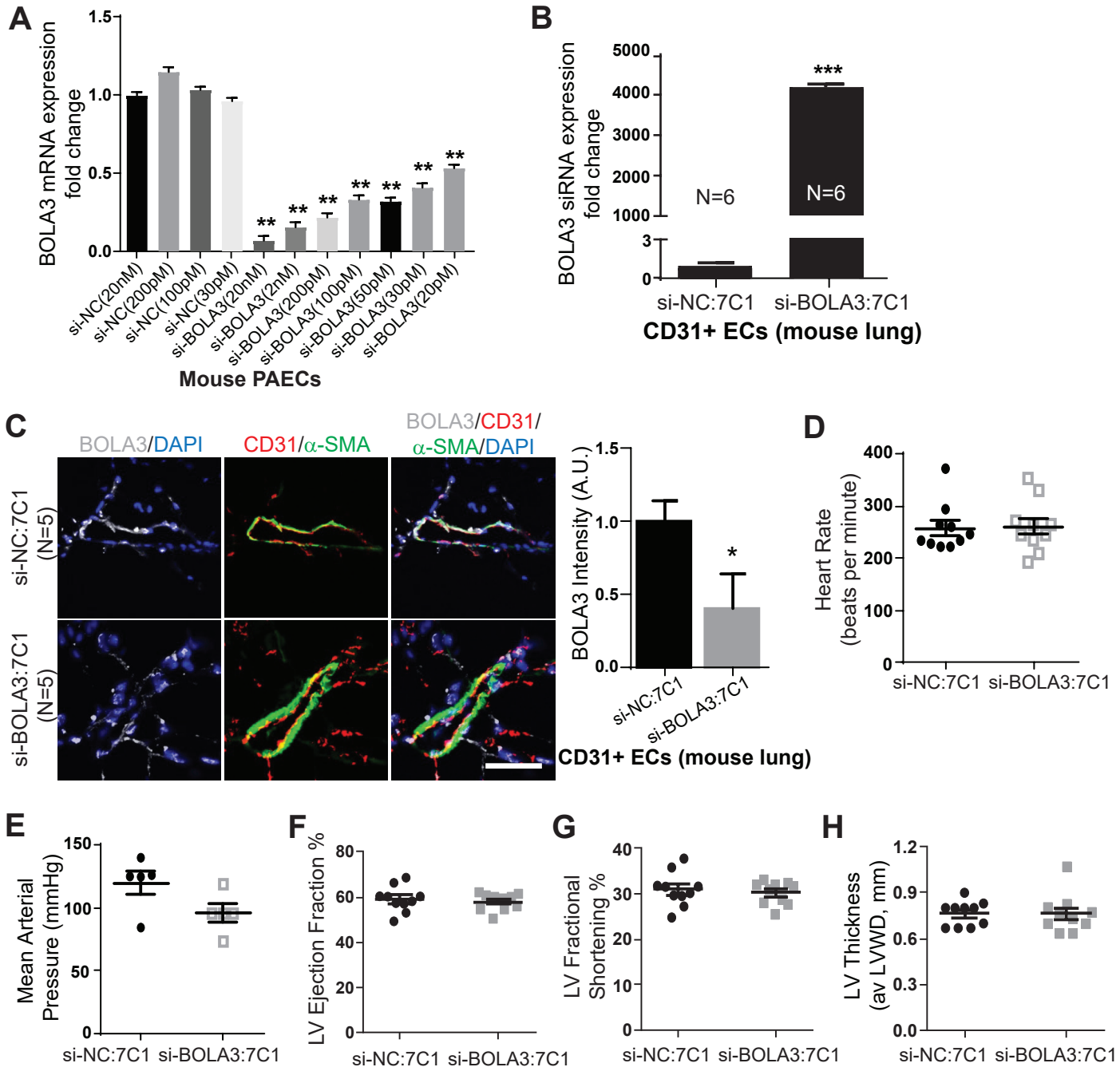

Yu et al. Figure S12

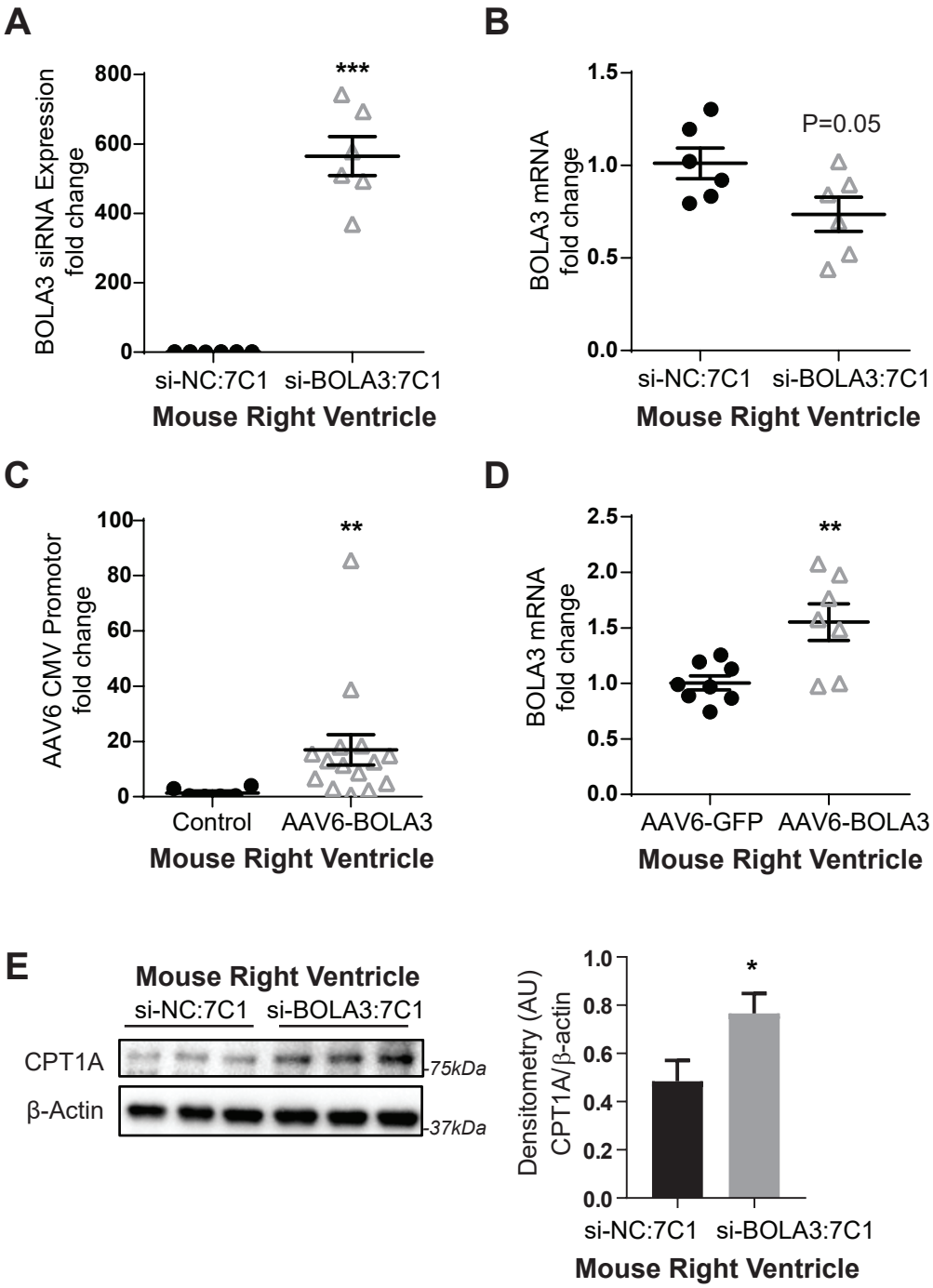

Yu et al. Figure S13

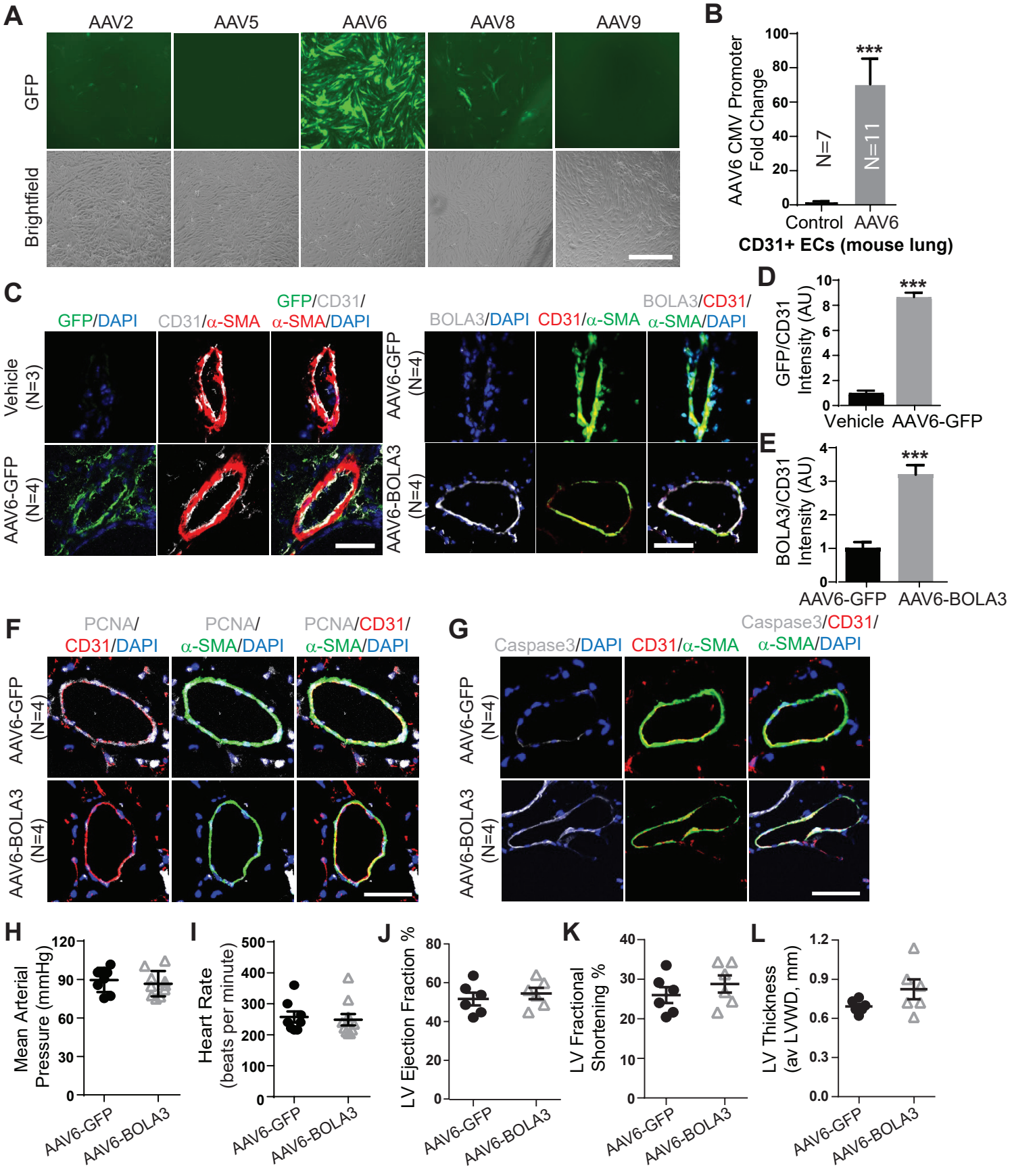

Yu et al. Figure S14

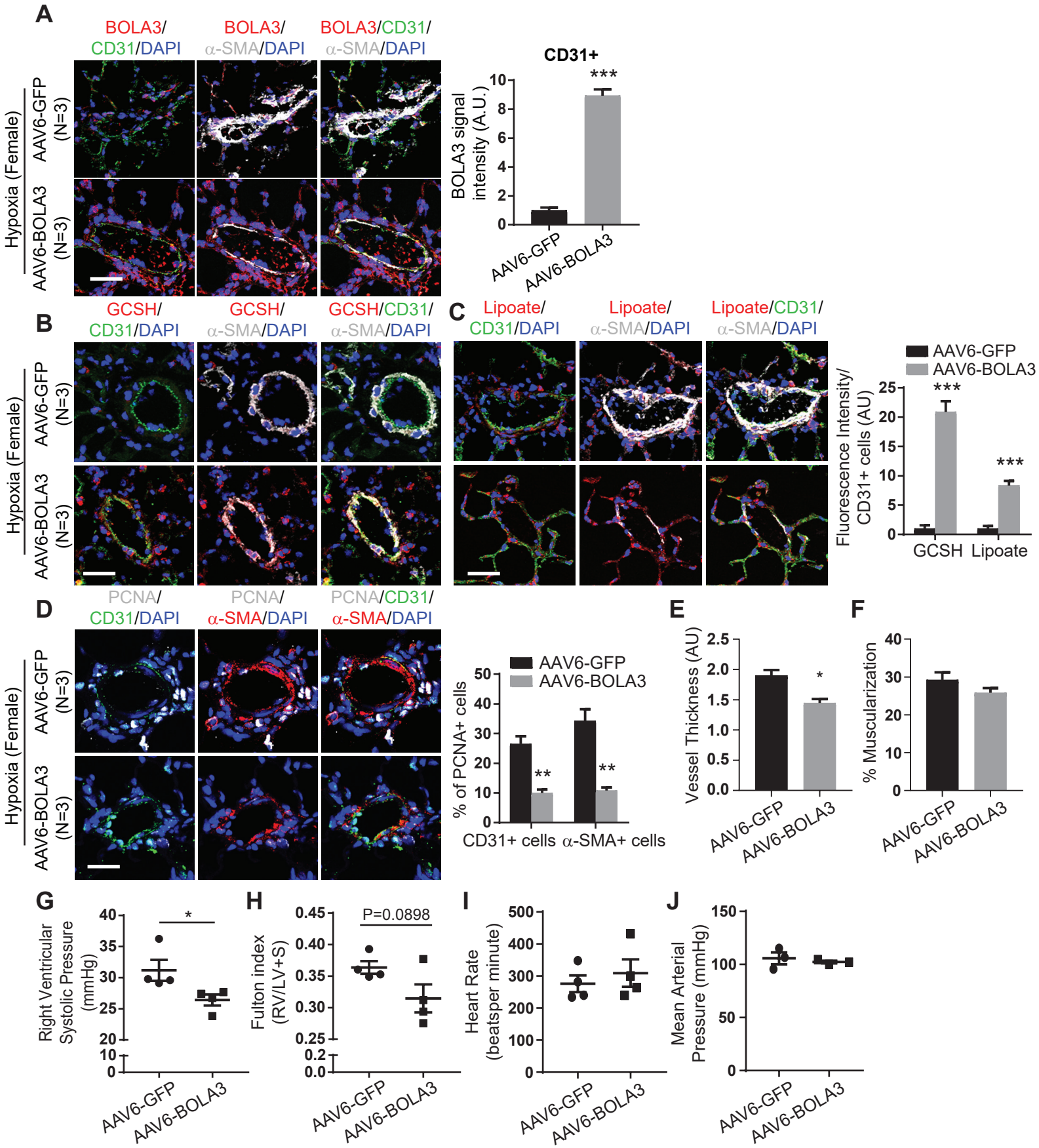

Yu et al. Figure S15

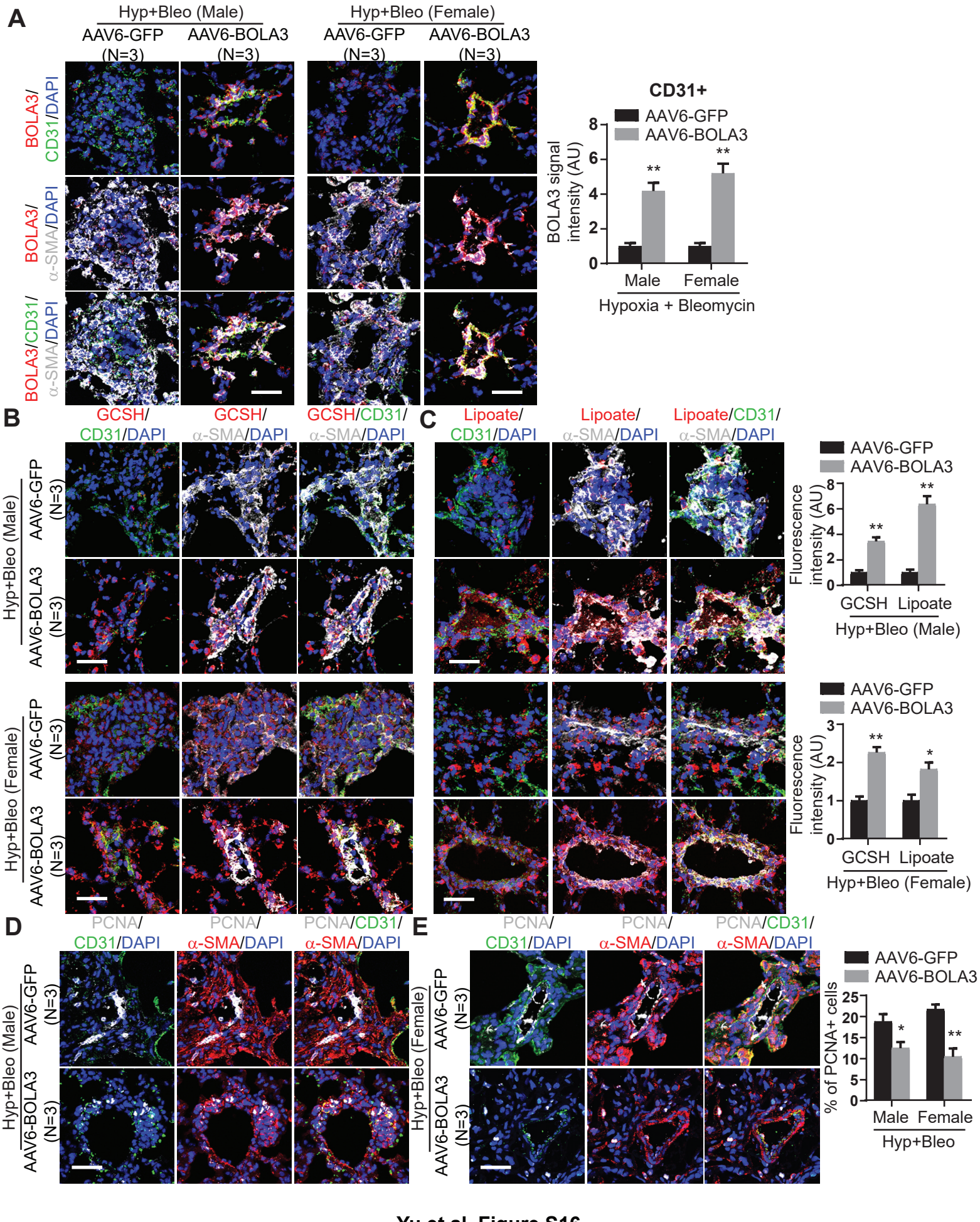

Yu et al. Figure S16

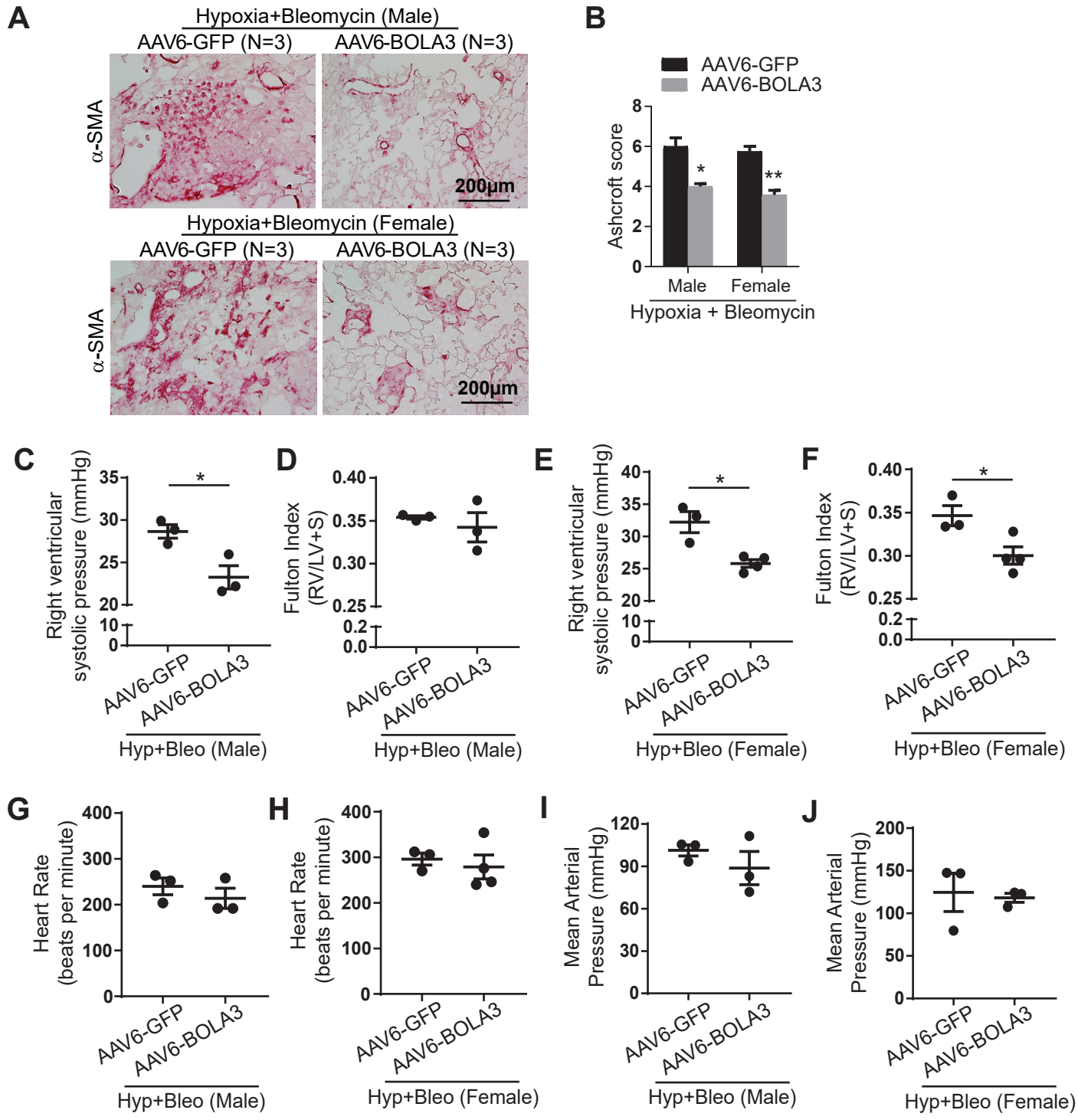

Yu et al. Figure S17

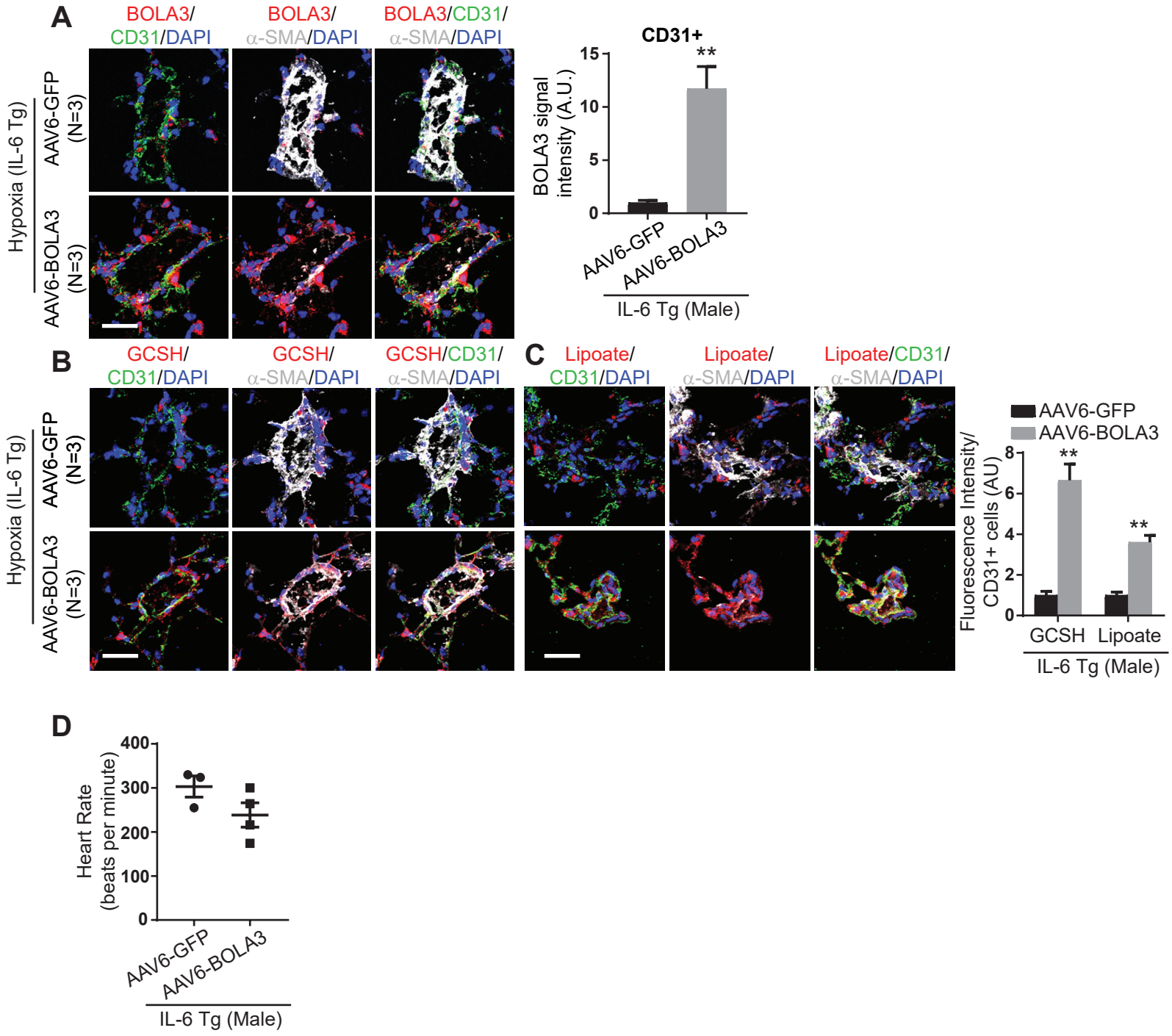

Yu et al. Figure S18

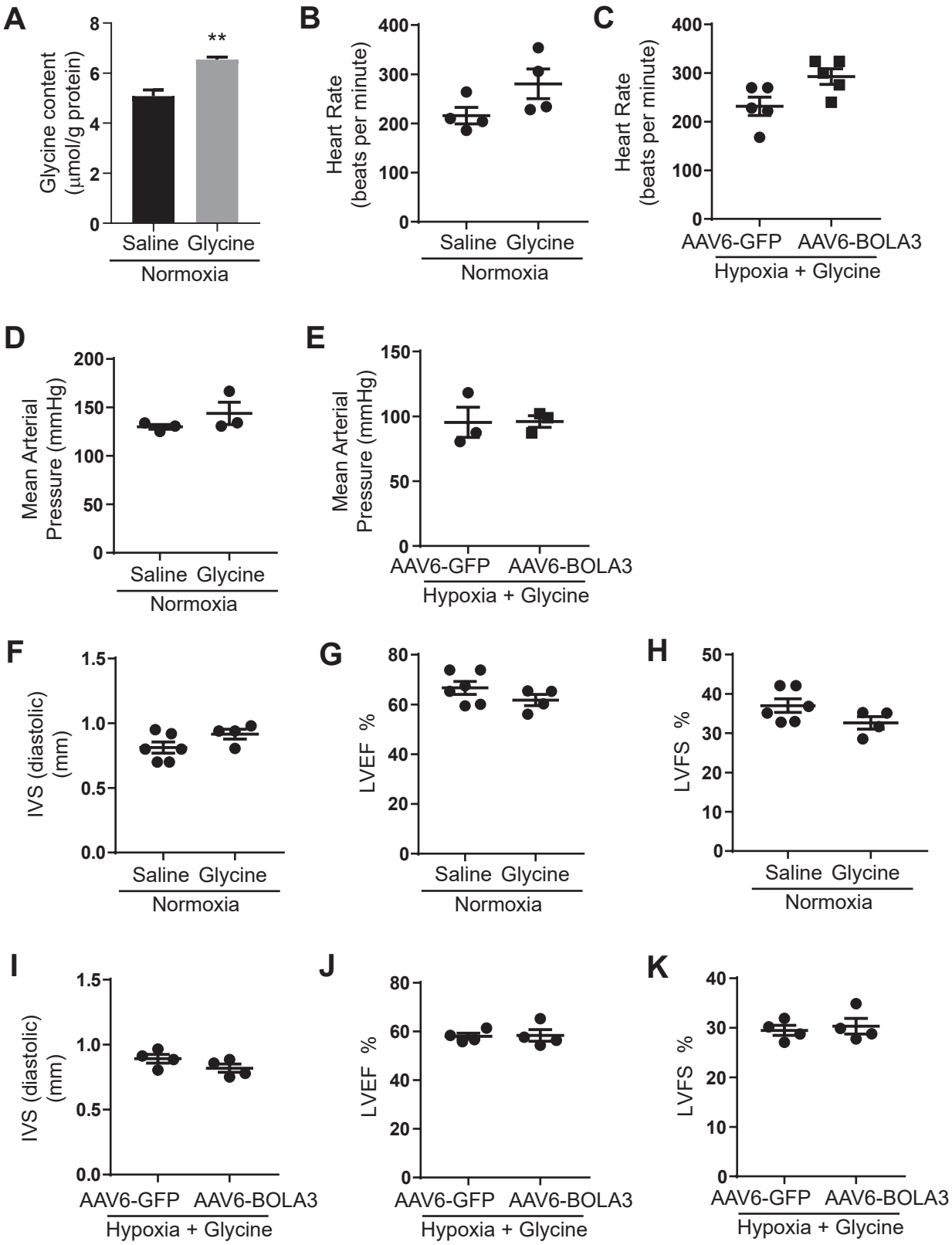

Yu et al. Figure S19

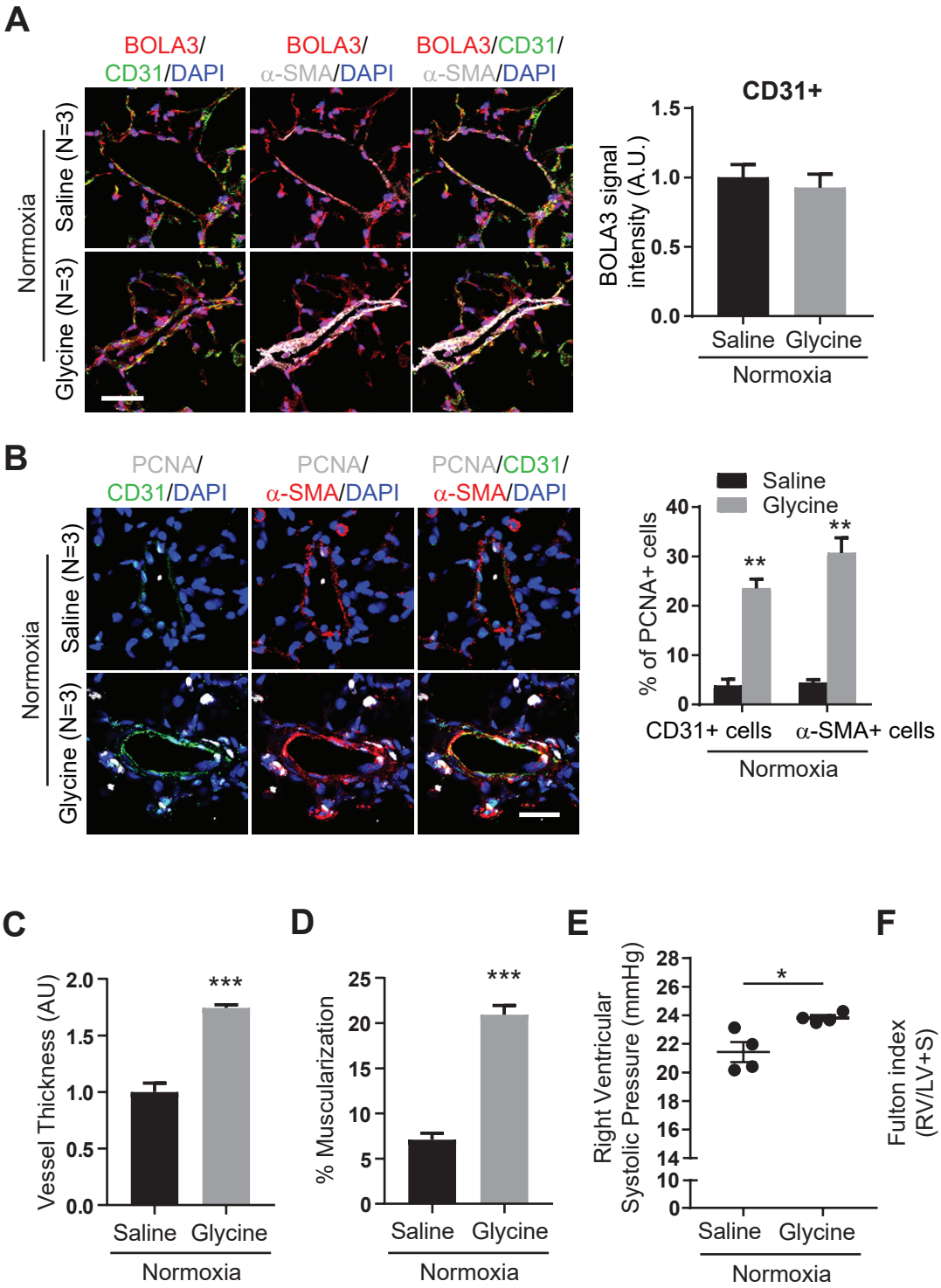

Yu et al. Figure S20

Supplemental Figure Legends

Supplemental Figure 1: Response of BOLA3 expression in a bleomycin+chronic hypoxia model of PH in mice. (A) Fluorescence microscopy of lung from male wildtype mice revealed reduced BOLA3 expression in endothelium (CD31 label) and smooth muscle (α-SMA label) when exposed to bleomycin and/or hypoxia, singly or in combination. Scale bar: 50μm. (B) By RT-qPCR, downstream transcript expression of COL1A and COL3A were up-regulated in whole lung when exposed to hypoxia alone and to a greater extent with bleomycin, singly or in combination. (C) A stepwise increase of right ventricular systolic pressure as measured by right heart catheterization was observed in wildtype mice exposed to bleomycin alone, hypoxia alone, and bleomycin+hypoxia in combination. (D) Right ventricular hypertrophy (Fulton index, RV/LV+S) was primarily increased with hypoxia, with or without bleomycin. (E) Fluorescence microscopy of lung from female wildtype mice revealed reduced BOLA3 expression in endothelium (CD31 label) and smooth muscle (α-SMA label) when exposed to bleomycin and/or hypoxia, singly or in combination. Scale bar: 50μm. (F-G) An increase of right ventricular systolic pressure as measured by right heart catheterization was observed in hypoxic female wildtype mice exposed to hypoxia, with or without bleomycin (F), while a stepwise increase was observed in Fulton index for mice exposed to bleomycin alone, hypoxia alone, and bleomycin+hypoxia in combination (G). (H) Via immunohistochemical staining of α-SMA of vascular smooth muscle and fibroblast cells, Ashcroft score revealed an increase of pulmonary parenchymal and pulmonary vascular fibrosis in bleomycin-exposed mice in normoxia and hypoxia. Scale bar: 200μm. In panel B, mean expression of control groups (Nx Control) was normalized to fold change of 1, to which relevant samples were compared (N = 3/group). In these experiments, unless indicated otherwise, N = 3-7 mice per group. Data represent mean ± SEM (*P < 0.05, **P < 0.01, ***P < 0.001, ****P < 0.0001, by two-way ANOVA).

Supplemental Figure 2: Response of BOLA3 expression in established PAH rat models and in cultured PAECs and PASMCs.

(A-B) Fluorescence microscopy of rat lung from monocrotaline-induced PH rats (A) or SU5416-hypoxic (SuHx) PH rats (B) vs. vehicle control revealed reduced BOLA3 expression in endothelium (CD31 label) and smooth muscle (α-SMA label). Scale bar: 50μm. N = 4-5 rats/group. (C) By RT-qPCR, exposure of cultured human PAECs to interleukin (IL)-1β resulted in no significant change of BOLA3 expression. (D) By RT-qPCR, siRNA-mediated knockdown of a panel of genes that have been genetically linked to PH did not alter BOLA3 expression in PAECs. (E) By RT-qPCR, BOLA3 expression was not altered by hypoxia in cultured human pulmonary artery smooth muscle cells (PASMCs). In all panels, mean expression of control groups (control, normoxia, si-NC) was normalized to fold change of 1, to which relevant samples were compared (N = 3/group). Data represent the mean ± SEM (**P < 0.01. ***P < 0.01, as calculated by two-tailed t-test when comparing two groups and one-way ANOVA in panel D).

Supplemental Figure 3: Quantification of Fe-S content by fluorescent sensor lentiviruses and efficiencies of BOLA3 knockdown and overexpression.

(A) As assessed by fluorescent signal after lentiviral delivery of Fe-S-dependent (GRX2, left) or Fe-S-independent (GCN4, right) sensors to human PAECs, BOLA3 knockdown decreased Fe-S integrity in human PAECs. Scale bars, 200μm. (B-C) By RT-qPCR, comparable lentiviral transgene delivery of GRX (B) and GCN (C) was achieved with siRNA knockdown of BOLA3 vs. control (NC), indicating the alteration of fluorescent signal was due to Fe-S levels and not differential sensor expression. (D-E) Via RT-PCR, robust alterations of BOLA3 mRNA expression were observed with knockdown (small-interfering RNA, siRNA) and forced expression (lentiviral BOLA3 transgene delivery) in human PAECs. Mean expression in controls (si-NC, LV-GFP) was normalized to a fold change of 1, to which relevant samples were compared (N = 3/group) by one-way ANOVA analysis. Data represent the mean ± SEM NS, P > 0.05, *P < 0.05, **P < 0.01).

Supplemental Figure 4: BOLA3 knockdown increases phosphorylation of PDK1, and its effects on PDH activity are reversed by dichloroacetate.

(A) By immunoblot and densitometry in human PAECs, phospho-PDK1 was increased by BOLA3 knockdown in normoxia and endogenously in hypoxia. (B) Dichloroacetate (DCA, 5mM) treatment for 24 hours increased PDH activity in hypoxia and reversed the decrease of PDH activity induced by BOLA3 knockdown. N = 3/group. Data represent the mean ± SEM (*P < 0.05, **P < 0.01, by two-way ANOVA).

Supplemental Figure 5: Exogenous glycine promotes PAEC proliferation and glycolytic gene expression.

(A) By immunoblot and densitometry, no expression changes in PAECs were observed in glycine dehydrogenase (GLDC) and serine hydroxymethyltransferase (SHMT1) after BOLA3 knockdown in normoxia or hypoxia. (B-C) By RT-qPCR, GCSH mRNA expression analysis confirmed effective knockdown and forced expression mediated by siRNA and lentiviral BOLA3 transgene delivery, respectively, in human PAECs. (D-E) By RT-qPCR, exogenous glycine increased transcript levels of the glycolytic genes, LDHA and PDK1. (F-G) Exogenous glycine increased PAEC proliferation, as measured by cell number (F) and BrdU incorporation (G). (H-J) Forced GCSH expression (LV-GCSH) reversed the alterations induced by knockdown of BOLA3 (si-BOLA3), including changes in glycine content (H) as well as LDHA (I) and PDK1 (J) expression. (K-L) Forced GCSH expression reversed the si-BOLA3-induced decrease in Complex I (K) and PDH (L) activity. In all panels, mean expression of control groups (si-NC, glycine 0mM, si-NC+LV-GFP in normoxia) was normalized to fold change of 1, to which relevant samples were compared (N = 3/group). Data represent the mean ± SEM (*P < 0.05, **P < 0.01, by one-way or two-way ANOVA, as indicated).

Supplemental Figure 6: MMDS2 primary human fibroblasts carrying homozygous missense mutations in BOLA3 carry defects in lipoylation and GCSH, resulting in increased glycine production.

(A) By immunoblot and densitometry, primary human fibroblasts carrying homozygous missense

mutations in BOLA3 (BOLA3 mut FB) displayed near complete abolishment of BOLA3 expression at the protein level and downstream lipoylated PDH as compared with wildtype human fibroblasts (WT FB). Significant but not full abolishment of GCSH expression was observed. (B-C) By RT-qPCR, BOLA3 (B) and GCSH (C) mRNA transcript expression was decreased but not fully abolished in mutant fibroblasts. (D-E) Glycine content in cell lysate (D) and cell media (E) was increased in mutant fibroblast cultures. In panels A-C, mean levels of wildtype human fibroblasts were normalized to fold change of 1, to which BOLA3 mutant fibroblasts were compared (N = 3 replicates/group). Data represent the mean ± SEM ((*P < 0.05, **P < 0.01, by two-tailed t test).

Supplemental Figure 7: BOLA3 deficiency activates PAEC glycolysis and fatty acid oxidation.
(A-D) Glycolysis (extracellular acidification rate, ECAR, A) and oxygen consumption rate (OCR, B) were measured in human PAECs by Seahorse assay during forced expression of HIF-2α vs. GFP control. While HIF-2α increased ECAR and decreased OCR, BOLA3 knockdown increased both baseline ECAR (C) and OCR (D) in control and HIF-dependent conditions. (E) BOLA3 knockdown in normoxic PAECs increased lactate levels in cell lysate, phenocopying the glycolytic state in hypoxia. BOLA3 knockdown in hypoxia further augmented lactate levels. (F-I) When measured during exposure to etomoxir (eto), an inhibitor of carnitine palmitoyl transferase (CPT1) and mitochondrial fatty acid oxidation, BOLA3 knockdown increased ECAR (F,H) but decreased OCR (G,I), N = 10-12 replicates/group. (J-K) BOLA3 knockdown in PAECs did not affect mRNA expression of key mitochondrial biogenesis genes nuclear respiratory factor 1 (NRF1) and transcription factor A, mitochondrial (TFAM). (L-M) BOLA3 knockdown specifically increased expression of the FAO enzyme carnitine palmitoyl transferase 1A (CPT1A) at the mRNA and protein levels. (N) When the fatty acid palmitate was used as the primary endothelial substrate, OCR was increased with BOLA3 knockdown but was reversed with etomoxir (N = 10-12 replicates/group). In panels J-L, mean expression of control group (Nx+si-NC) was normalized to fold change of 1, to which relevant samples were compared (N >

3/group). Data represent the mean ± SEM (NS, P > 0.05, *P < 0.05, **P < 0.01, by two-tailed t-test or two-way ANOVA, as indicated).

Supplemental Figure 8: BOLA3 deficiency drives the production of reactive oxygen species.

(A) BOLA3 knockdown increased proton leak of the electron transport chain as measured by OCR after oligomycin exposure. (B-C) BOLA3 knockdown increased mitochondrial O_2^- production as quantified by fluorescence microscopy of Mitosox red label. (D-E) BOLA3 knockdown increased cellular H_2O_2 production and oxidative DNA damage, as assessed by Amplex red H_2O_2 assay and 8-oxoguanine staining. (F-H) In hypoxia, forced BOLA3 expression reduced mitochondrial O_2^- production (as measured by Mitosox red labeling, F); cellular H_2O_2 production (as assessed by Amplex red assay, G); and oxidative DNA damage (as assessed by 8-oxoguanine staining, H). N = 3/group. Data represent the mean ± SEM (*P < 0.05, **P < 0.01, by two-way ANOVA). Scale bar, 20μm.

Supplemental Figure 9: BOLA3 deficiency controls PAEC pathophenotypes, some of which can be reversed with forced expression of GCSH.

(A) As reflected by cell count, BOLA3 knockdown increased PAEC proliferation in normoxia and hypoxia (N > 3/group). (B) Via *in vivo* Matrigel plug angiogenesis assay, human PAECs transfected with BOLA3 siRNA or scrambled control were mixed with matrigel and placed subcutaneously into SCID mice (N = 3 mice/group). After 5 days, matrigel plugs were harvested, and hemoglobin was quantified as a surrogate measure of functional angiogenesis and transport of blood to the matrigel. Plugs with BOLA3-deficient PAECs displayed lower levels of hemoglobin. Hemoglobin content of control group (si-NC) was normalized to fold change of 1, to which si-BOLA3 samples were compared. (C) Matrigel plugs were sectioned and stained by fluorescence microscopy for CD31+ endothelial cells (red), as a reflection of angiogenic persistence (N = 3/group). Plugs with BOLA3-deficient PAECs displayed lower levels of CD31+ endothelial cells 5 days post-subcutaneous placement. (D) In cultured human PAECs, forced GCSH expression (LV-GCSH) reversed the alterations induced by knockdown of BOLA3 (si-BOLA3),

including changes in BrdU incorporation (N = 6/group) (D) and EDN1 expression (N = 3/group) (E) but not apoptotic caspase 3/7 activity (N = 8-12/group) (F). Data represent mean ± SEM (*P < 0.05, **P < 0.01, by t-test or ANOVA as indicated). Scale bars, 200 μm.

Supplemental Figure 10: Replication of key experiments using a separate set of siRNAs and scrambled control oligonucleotides. (A-K) In cultured PAECs, key experimental results were replicated using a separate siRNA specific for BOLA3 compared with a separate scrambled control siRNA. (L-N) In cultured PAECs, key experimental results were replicated using a separate siRNA specific for GCSH compared with a separate scrambled control siRNA. In (A, D, J, K, L, M), mean expression of control group (Nx+si-NC) was normalized to fold change of 1, to which relevant samples were compared (N > 3/group). Data represent mean ± SEM (*P < 0.05, **P < 0.01, by two-way ANOVA).

Supplemental Figure 11: Pulmonary vascular lipoate and GCSH levels are down-regulated in Group 1 and Group 3 PH patients.

(A-B) Fluorescence microscopy of lung from human Group 1 PAH (A) and Group 3 PH (B) patients as compared with non-PH individuals revealed reduced lipoate and GCSH expression, including in the pulmonary arterial endothelium (CD31 label). Scale bar: 50μm. In all panels, N = 6-8/group. Data represent the mean ± SEM (***P < 0.001, by two-tailed t test).

Supplemental Figure 12: Left ventricular function, systemic blood pressure, and heart rates were unchanged in mice administered si-BOLA3:7C1 or si-NC:7C1 nanoparticles.

(A) RNA expression of BOLA3 in mouse PAECs treated with BOLA3 siRNA used in 7C1 nanoparticle formulation at a concentration range of 20ρM-20nM (N = 3/group). Mean levels of controls (si-NC) were normalized to fold change of 1, to which relevant samples were compared. (B) By RT-qPCR, BOLA3

siRNA expression was detected in mouse lung CD31+ cells after 28 days of serial administration. Here, the minimum level of PCR detectability was normalized to a fold change of 1, to which all samples were compared. (C) si-BOLA3:7C1 nanoparticles reduced pulmonary endothelial BOLA3 expression by *in situ* staining in mouse lung tissues. (D) Delivery of si-BOLA3:7C1 did not alter mouse heart rate compared with si-NC:7C1. (E) As measured by non-invasive tail cuff plethysmography, mean arterial pressure was unchanged in mice administered si-BOLA3:7C1 compared with si-NC:7C1 nanoparticles. In panels B-E, N = 5-6 mice/group. (F-H) By transthoracic echocardiography, left ventricular (LV) ejection fraction (F), fractional shortening (G), and average of left ventricular anterior and posterior wall dimensions (av IVWD, H) were unchanged in mice administered si-BOLA3:7C1 compared with si-NC:7C1 nanoparticles (N = 10 mice/group). Data represent the mean ± SEM (*P < 0.05, **P < 0.01, ***P < 0.001, by two-tailed t-test or ANOVA, as indicated). Scale bars, 50μm.

Supplemental Figure 13: Right ventricular BOLA3 expression in mice receiving siBOLA3:7C1 or AAV6-BOLA3 treatment.

(A) Detection of BOLA3 siRNA in right ventricular tissue of mice after serial administration of siBOLA3:7C1 nanoparticles (N = 6/group). (B) As measured by RT-qPCR, right ventricular BOLA3 expression decreased modestly after treatment of siBOLA3:7C1 vs. siNC:7C1 in normoxic mice (N = 6/group). (C) Detection of AAV6 CMV promoter expression in right ventricles of mice treated with either PBS (control) or AAV-BOLA3 (N = 15/group). (D) As measured by RT-qPCR, right ventricular BOLA3 expression was modestly increased after delivery of AAV6-BOLA3 in chronically hypoxic mice (N = 8/group). (E) By immunoblot and densitometry, CPT1A expression was augmented in the RV after si-BOLA3:7C1 treatment as compared with si-NC:7C1 (N = 3/group). In (A,C), the minimum level of PCR detectability was normalized to a fold change of 1, to which all samples were compared. In (B,D), mean expression of control groups (si-NC:7C1, AAV6-GFP) were normalized to fold change of 1, to which relevant samples were compared. Data represent the mean ± SEM (*P < 0.05, **P < 0.01, ***P < 0.001).

Supplemental Figure 14: Transduction efficiency of AAV6-GFP and AAV6-BOLA3 in mouse lung vessels.

(A) By fluorescent and brightfield microscopy, AAV6-GFP displayed the highest expression in mouse PAECs 3 days after transduction. (B) Detection of AAV6 CMV promotor expression in lung CD31+ cells from hypoxic mice administered either AAV6-GFP or AAV6-BOLA3. In panels A-B, N = 7-11/group. (C-E) AAV6-GFP increased GFP expression, and AAV6-BOLA3 increased BOLA3 expression in mouse pulmonary vasculature, particularly in CD31+ endothelial cells. (F-G) AAV6-BOLA3 reduced PCNA (F) but enhanced cleaved caspase 3 (CC-3) expression (G) in both CD31+ and α-SMA+ cells in hypoxic mouse pulmonary vessels. In panels C-G, N = 3-4/group. (H-I) Mean arterial pressure and heart rate were unchanged in hypoxic mice received AAV-BOLA3 compared with AAV-GFP (N = 8-10 mice/group). (J-L) By echocardiography, left ventricular ejection fraction, fractional shortening, and left ventricular wall thickness were unchanged in hypoxic mice administered AAV-BOLA3 compared with AAV-GFP (N = 6 mice/group). Data represent the mean± SEM (***P < 0.001, by two-tailed t test). Scale bars, 50μm.

Supplemental Figure 15: Forced expression of pulmonary vascular BOLA3 prevents PH in female hypoxic mice.

(A) As assessed by fluorescent microscopy, AAV6-BOLA3 was effectively delivered to the pulmonary vasculature of female mice, particularly in CD31+ endothelial cells. (B-C) After exposure to hypoxia for 3 weeks, AAV6-BOLA3 increased GCSH and lipoate expression, particularly in CD31+ endothelial cells. (D) AAV6-BOLA3 reduced PCNA in both CD31+ and α-SMA+ cells in mouse pulmonary vessels. (E-F) AAV6-BOLA3 reduced pulmonary vessel thickness and muscularization, as assessed by α-SMA staining. (G-H) AAV6-BOLA3 reduced right ventricular systolic pressure (G) as measured by right heart catheterization, accompanied by a trend toward improvement of right ventricular hypertrophy (Fulton

index, RV/LV+S) (H). (I-J) Delivery of AAV6-BOLA3 did not alter mouse heart rate (I) or mean arterial pressure systemically (J) compared with AAV6-GFP. In panels A and C, mean expression of control group (AAV6-GFP) was normalized to fold change of 1, to which relevant samples were compared. Data represent the mean ± SEM (*P < 0.05, **P < 0.01, ***P < 0.001, by two-tailed t test). Scale bars, 50μm. In these experiments, unless indicated otherwise, N = 3-4 mice per group.

Supplemental Figure 16: Forced expression of pulmonary vascular BOLA3 prevents lipoate-GCSH-PCNA dysregulation in male and female mice exposed to bleomycin and hypoxia.

(A) As assessed by fluorescent microscopy, AAV6-BOLA3 was effectively delivered to the pulmonary vasculature of male and female mice exposed to bleomycin and hypoxia, particularly in CD31+ endothelial cells. (B-C) After bleomycin exposure and 3 weeks of hypoxia, AAV6-BOLA3 increased pulmonary vascular GCSH and lipoate expression as compared with AAV6-GFP. Notably, due to the fibrotic distortion of the pulmonary vascular architecture, determination of endothelial-specific expression was not possible. (D-E) AAV6-BOLA3 reduced PCNA in pulmonary vascular cells in fibrotic mouse pulmonary vessels of male and female hypoxia+bleomycin mice. In panels A-C, mean expression of control group (AAV6-GFP) was normalized to fold change of 1, to which relevant samples were compared. Data represent the mean ± SEM (*P < 0.05, **P < 0.01, by two-tailed t test). Scale bars, 50μm. In these experiments, unless indicated otherwise, N = 3-4 mice per group.

Supplemental Figure 17: Forced expression of pulmonary vascular BOLA3 prevents PH in male and female mice exposed to bleomycin and hypoxia.

(A-D) Via α-SMA immunohistochemical staining of vascular smooth muscle and fibroblast cells, in both male and female mice exposed to bleomycin and hypoxia, AAV6-BOLA3 reduced pulmonary parenchymal and vascular fibrosis and remodeling, as assessed by α-SMA staining and Ashcroft score. (C-F) AAV6-BOLA3 reduced right ventricular systolic pressure (C,E) as measured by right heart

catheterization, accompanied by improved right ventricular hypertrophy (Fulton index, RV/LV+S) in females (F) but not males (D). (G-J) In either males or females, delivery of AAV6-BOLA3 did not alter mouse heart rate (G-H) or mean arterial pressure systemically (I-J) as compared with AAV6-GFP. Data represent the mean ± SEM (*P < 0.05, **P < 0.01, by two-tailed t test). Scale bars, 50μm. In these experiments, unless indicated otherwise, N = 3-4 mice per group.

Supplemental Figure 18: Forced expression of pulmonary vascular BOLA3 prevents lipoate-GCSH-PCNA dysregulation in hypoxic IL-6 transgenic mice.

(A) As assessed by fluorescent microscopy, AAV6-BOLA3 was effectively delivered to the pulmonary vasculature of male IL-6 transgenic (IL-6 Tg) mice, particularly in CD31+ endothelial cells. (B-C) After exposure to 3 weeks of hypoxia, AAV6-BOLA3 increased GCSH and lipoate expression, particularly in CD31+ endothelial cells. (D) Delivery of AAV6-BOLA3 did not alter mouse heart rate in IL-6 Tg mice as compared with AAV6-GFP. In panels A and C, mean expression of control group (AAV6-GFP) was normalized to fold change of 1, to which relevant samples were compared. Data represent the mean ± SEM (**P < 0.01, by two-tailed t test). Scale bars, 50μm. In these experiments, unless indicated otherwise, N = 3-4 mice per group.

Supplemental Figure 19: Left ventricular function, systemic blood pressure, and heart rates were unchanged in mice supplemented chronically with glycine.

(A) As quantified by fluorometric assay, glycine supplementation successfully increased whole lung glycine content in normoxic wildtype mice (N = 5 mice/group). (B-C) Mouse heart rate was not altered by glycine supplementation as compared with saline (B) and was not altered by AAV6-BOLA3 as compared with AAV6-GFP in hypoxic conditions with glycine supplementation (C). (D-E) As measured by non-invasive tail cuff plethysmography, glycine supplementation did not alter systemic mean arterial pressure compared with saline (D) and did not allow AAV6-BOLA3 to alter systemic mean arterial pressure significantly as compared with AAV6-GFP (E). (F-H) By transthoracic echocardiography,

interventricular septal diastolic thickness (IVS diastolic, F), left ventricular ejection fraction (LVEF %, G), and left ventricular fractional shortening (LVFS %, H) were unchanged in mice administered glycine. (I-K) By transthoracic echocardiography, interventricular septal diastolic thickness (I), left ventricular ejection fraction (J), and left ventricular fractional shortening (K) were unchanged in mice administered AAV6-BOLA3 versus AAV6-GFP during hypoxia with glycine supplementation. Data represent the mean ± SEM (**P < 0.01, by two-tailed t test). In these experiments, unless indicated otherwise, N = 3-6 mice per group.

Supplemental Figure 20: In normoxic mice, glycine supplementation induces a modest increase of pulmonary vascular proliferation, remodeling, and RVSP.

(A) As assessed by fluorescent microscopy, pulmonary vascular BOLA3 expression was not altered with glycine supplementation in normoxic wildtype mice. Mean expression of control group (PBS) was normalized to fold change of 1, to which the glycine group was compared. (B) Glycine supplementation increased the proliferation marker PCNA in CD31+ and α-SMA+ cells in small pulmonary arterioles of normoxic mice. (C-D) Glycine supplementation increased pulmonary vessel thickness and muscularization, as assessed by α-SMA staining. (E-F) Glycine supplementation modestly increased right ventricular systolic pressure (E) accompanied by negligible changes in right ventricular hypertrophy (Fulton index, RV/LV+S) (F). Data represent the mean ± SEM (NS, P > 0.05, *P < 0.05, **P < 0.01, ***P<0.001, by two-tailed t test). In these experiments, unless indicated otherwise, N = 3-4 mice per group.

Supplemental References

1. Haack TB, Rolinski B, Haberberger B, Zimmermann F, Schum J, Strecker V, Graf E, Athing U, Hoppen T, Wittig I, Sperl W, Freisinger P, Mayr JA, Strom TM, Meitinger T and Prokisch H. Homozygous missense mutation in BOLA3 causes multiple mitochondrial dysfunctions syndrome in two siblings. *J Inherit Metab Dis*. 2013; 36:55-62.
2. Chan SY, Zhang YY, Hemann C, Mahoney CE, Zweier JL and Loscalzo J. MicroRNA-210 controls mitochondrial metabolism during hypoxia by repressing the iron-sulfur cluster assembly proteins ISCU1/2. *Cell Metab*. 2009; 10:273-284.
3. Kondo K, Kim WY, Lechpammer M and Kaelin WG, Jr. Inhibition of HIF2alpha is sufficient to suppress pVHL-defective tumor growth. *PLoS Biol*. 2003; 1:E83.
4. Bertero T, Cotrill KA, Lu Y, Haeger CM, Dieffenbach P, Annis S, Hale A, Bhat B, Kaimal V, Zhang YY, Graham BB, Kumar R, Saggar R, Saggar R, Wallace WD, Ross DJ, Black SM, Fratz S, Fineman JR, Vargas SO, Haley KJ, Waxman AB, Chau BN, Fredenburgh LE and Chan SY. Matrix remodeling promotes pulmonary hypertension through feedback mechanoactivation of the YAP/TAZ-miR-130/301 circuit *Cell Rep*. 2015; 13:1016-1032.
5. Bertero T, Cottrill KA, Annis S, Bhat B, Gochuico BR, Osorio JC, Rosas I, Haley KJ, Corey KE, Chung RT, Nelson Chau B and Chan SY. A YAP/TAZ-miR-130/301 molecular circuit exerts systems-level control of fibrosis in a network of human diseases and physiologic conditions. *Sci Rep*. 2015; 5:18277.
6. Bertero T, Lu Y, Annis S, Hale A, Bhat B, Saggar R, Saggar R, Wallace WD, Ross DJ, Vargas SO, Graham BB, Kumar R, Black SM, Fratz S, Fineman JR, West JD, Haley KJ, Waxman AB, Chau BN, Cottrill KA and Chan SY. Systems-level regulation of microRNA networks by miR-130/301 promotes pulmonary hypertension. *J Clin Invest*. 2014; 124:3514-3528.
7. Bertero T, Oldham WM, Cottrill KA, Pisano S, Vanderpool RR, Yu Q, Zhao J, Tai Y, Tang Y, Zhang YY, Rehman S, Sugahara M, Qi Z, Gorcsan J, 3rd, Vargas SO, Saggar R, Saggar R, Wallace WD, Ross DJ, Haley KJ, Waxman AB, Parikh VN, De Marco T, Hsue PY, Morris A, Simon MA, Norris KA, Gaggioli C, Loscalzo J, Fessel J and Chan SY. Vascular stiffness mechanoactivates YAP/TAZ-dependent glutaminolysis to drive pulmonary hypertension. *J Clin Invest*. 2016; 126:3313-3335.
8. Hoff KG, Culler SJ, Nguyen PQ, McGuire RM, Silberg JJ and Smolke CD. In vivo fluorescent detection of Fe-S clusters coordinated by human GRX2. *Chem Biol*. 2009; 16:1299-1308.
9. White K, Lu Y, Annis S, Hale AE, Chau BN, Dahlman JE, Hemann C, Opotowsky AR, Vargas SO, Rosas I, Perrella MA, Osorio JC, Haley KJ, Graham BB, Kumar R, Saggar R, Saggar R, Wallace WD, Ross DJ, Khan OF, Bader A, Gochuico BR, Matar M, Polach K, Johannessen NM, Prosser HM, Anderson DG, Langer R, Zweier JL, Bindoff LA, Systrom D, Waxman AB, Jin RC and Chan SY. Genetic and hypoxic alterations of the microRNA-210-ISCU1/2 axis promote iron-sulfur deficiency and pulmonary hypertension. *EMBO Mol Med*. 2015; 7:695-713.
10. Nemkov T, Hansen KC and D'Alessandro A. A three-minute method for high-throughput quantitative metabolomics and quantitative tracing experiments of central carbon and nitrogen pathways. *Rapid Commun Mass Spectrom*. 2017; 31:663-673.
11. Passaniti A, Taylor RM, Pili R, Guo Y, Long PV, Haney JA, Pauly RR, Grant DS and Martin GR. A simple, quantitative method for assessing angiogenesis and antiangiogenic agents using reconstituted basement membrane, heparin, and fibroblast growth factor. *Lab Invest*. 1992; 67:519-528.
12. Chen Z, Lai TC, Jan YH, Lin FM, Wang WC, Xiao H, Wang YT, Sun W, Cui X, Li YS, Fang T, Zhao H, Padmanabhan C, Sun R, Wang DL, Jin H, Chau GY, Huang HD, Hsiao M and Shyy JY. Hypoxia-responsive miRNAs target argonaute 1 to promote angiogenesis. *J Clin Invest*. 2013; 123:1057-1067.
13. Bertero T, Cottrill K, Krauszman A, Lu Y, Annis S, Hale A, Bhat B, Waxman AB, Chau BN, Kuebler WM and Chan SY. The microRNA-130/301 family controls vasoconstriction in pulmonary hypertension. *J Biol Chem*. 2014; 290:2069-2085.

14. Gille T, Didier M, Rotenberg C, Delbrel E, Marchant D, Sutton A, Dard N, Haine L, Voituron N, Bernaudin JF, Valeyre D, Nunes H, Besnard V, Boncoeur E and Planes C. Intermittent Hypoxia Increases the Severity of Bleomycin-Induced Lung Injury in Mice. *Oxid Med Cell Longev*. 2018; 2018:1240192.
15. Steiner MK, Syrkina OL, Kolliputi N, Mark EJ, Hales CA and Waxman AB. Interleukin-6 overexpression induces pulmonary hypertension. *Circ Res*. 2009; 104:236-244.
16. Graham BB, Chabon J, Kumar R, Kolosionek E, Gebreab L, Debella E, Edwards M, Diener K, Shade T, Bifeng G, Bandeira A, Butrous G, Jones K, Geraci M and Tuder RM. Protective role of IL-6 in vascular remodeling in Schistosoma pulmonary hypertension. *Am J Respir Cell Mol Biol*. 2013; 49:951-959.
17. Dahlman JE, Barnes C, Khan OF, Thiriot A, Jhunjunwala S, Shaw TE, Xing Y, Sager HB, Sahay G, Speciner L, Bader A, Bogorad RL, Yin H, Racie T, Dong Y, Jiang S, Seedorf D, Dave A, Singh Sandhu K, Webber MJ, Novobrantseva T, Ruda VM, Lytton-Jean AK, Levins CG, Kalish B, Mudge DK, Perez M, Abezgauz L, Dutta P, Smith L, Charisse K, Kieran MW, Fitzgerald K, Nahrendorf M, Danino D, Tuder RM, von Andrian UH, Akinc A, Panigrahy D, Schroeder A, Koteliansky V, Langer R and Anderson DG. In vivo endothelial siRNA delivery using polymeric nanoparticles with low molecular weight. *Nat Nanotechnol*. 2014; 9:648-655.
18. Wang Z, Zhu T, Qiao C, Zhou L, Wang B, Zhang J, Chen C, Li J and Xiao X. Adeno-associated virus serotype 8 efficiently delivers genes to muscle and heart. *Nat Biotechnol*. 2005; 23:321-328.
19. Xue J, Lin H, Bean A, Tang Y, Tan J, Tuan RS and Wang B. One-Step Fabrication of Bone Morphogenetic Protein-2 Gene-Activated Porous Poly-L-Lactide Scaffold for Bone Induction. *Mol Ther Methods Clin Dev*. 2017; 7:50-59.
20. Ashcroft T, Simpson JM and Timbrell V. Simple method of estimating severity of pulmonary fibrosis on a numerical scale. *J Clin Pathol*. 1988; 41:467-470.